Improving ECC Ozonesonde Data Quality: Assessment of Current Methods and Outstanding Issues

David W. Tarasick[1], **Herman G. J. Smit[2]**, **Anne M. Thompson[3]**, **Gary A. Morris[4]**, **Jacquelyn C. Witte[5]**, **Jonathan Davies[1]**, **Tatsumi Nakano[6]**, **Roeland Van Malderen[7]**, **Ryan M. Stauffer[8]**, **Bryan J. Johnson[9]**, **Rene Stübi[10]**, **Samuel J. Oltmans[9]**, and **Holger Vömel[11]**

[1]Air Quality Research Division, Environment and Climate Change Canada, Downsview, ON, Canada, [2]Institute for Energy and Climate Research: Troposphere (IEK-8), Research Centre Juelich (FZJ), Juelich, Germany, [3]NASA Goddard Space Flight Center, Greenbelt, MD, USA, [4]St. Edward's University, Austin, TX, USA, [5]Earth Observing Laboratory, National Center for Atmospheric Research, Boulder, CO, USA, [6]Japan Meteorological Agency, Tokyo, Japan, [7]Royal Meteorological Institute of Belgium, Brussels, Belgium, [8]NASA Goddard Space Flight Center and University of Maryland Earth System Science Interdisciplinary Center, MD, USA, [9]NOAA/ESRL Global Monitoring Division, Boulder, CO, USA, [10]MeteoSwiss Aerological Station, Federal Office of Meteorology and Climatology MeteoSwiss, Payerne, Switzerland, [11]National Center for Atmospheric Research, Boulder, CO, USA

Abstract We review the current state of knowledge of ozonesonde uncertainty and bias, with reference to recent developments in laboratory and field experiments. In the past 20 years ozonesonde precision has improved by a factor of 2, primarily through the adoption of strict standard operating procedures. The uncertainty budget for the ozone partial pressure reading has contributions from stoichiometry, cell background current, pump efficiency and temperature, sensing solution type, and volume. Corrections to historical data for known issues may reduce biases but simultaneously introduce additional uncertainties. This paper describes a systematic approach to quantifying these uncertainties by considering the physical and chemical processes involved and attempts to place our estimates on a firm theoretical or empirical footing. New equations or tables for ozone/iodine conversion efficiency, humidity and temperature corrections to pump flow rate, and altitude-dependent pump flow corrections are presented, as well as detailed discussion of stoichiometry and conversion efficiencies. The nature of the so-called "background current" is considered in detail. Two other factors particularly affecting past measurements, uncertainties and biases in the pressure measurement, and the comparison of sonde profiles to spectrophotometric measurements of total column ozone, are also discussed. Several quality assurance issues remain, but are tractable problems that can be addressed with further research. This will be required if the present goal of better than 5% overall uncertainty throughout the global ozonesonde network is to be achieved.

Plain Language Summary Ozonesondes are a stable reference for the global ozone observing network, making relatively inexpensive, accurate measurements of ozone from the ground to 30 km, with high vertical resolution, for more than 50 years. Ozonesonde data are used extensively for validation of satellite ozone measurements, models, and for trend analyses. The current state of knowledge of ozonesonde uncertainty and bias is reviewed, and a systematic approach to quantifying these uncertainties by considering the physical and chemical processes involved is presented. While ozonesonde precision has improved through the adoption of strict standard operating procedures, further improvement is possible with further research, toward a goal of less than 5% overall uncertainty throughout the global network.

1. Introduction

Ozonesondes are the backbone of the global ozone observing network, making relatively inexpensive, accurate measurements of ozone from the ground to 30 km, with high vertical resolution (~100 m), for more than 50 years. Ozonesonde data are used extensively for validation of satellite ozone data products, and are also part of merged satellite data sets and climatologies that are used for trend analyses and as a priori data for satellite retrievals. The importance of electrochemical concentration cell (ECC) sondes for trend

analyses and as a transfer standard and stable reference for satellite validation demands better quantification of their uncertainties.

Over the past several decades monitoring of global ozone has been carried out using observations from satellites, ground-based photometers, balloon-borne ozonesondes, and lidar (e.g., Logan, 1994; SPARC-IOC-GAW, 1998; Tarasick et al., 2019b; Terao & Logan, 2007; Thompson et al., 2003; WMO, 2014; Zerefos et al., 2009), as well as commercial aircraft (e.g., Petzold et al., 2015; Thouret et al., 2006).

While trends of total and stratospheric ozone can be derived from ground-based spectrometer and satellite results, only ozonesondes and (where they exist) lidars can supply accurate, well-resolved profiles (to 100 m) throughout both the troposphere and lower-mid stratosphere. Ozonesondes have an advantage over lidar in being able to measure ozone in cloudy or rainy conditions. Otherwise, lidars provide better temporal coverage, but there are unfortunately only a handful of sites that measure routinely. Sondes are less technically complex and have less-intense labor requirements. Thus, they are much more frequently deployed in routine operations and so constitute the principal source of trend-quality long-term records of ozone profiles below about 18 km. As a data source that is also independent of ground-based spectrometers, ozonesonde measurements have been extensively used for trend analyses (Bojkov & Fioletov, 1997; Fioletov et al., 1997; Harris et al., 2015; Lin et al., 2014; Logan, 1994; Logan et al., 1999, 2012; Oltmans et al., 2006, 2013; Randel & Thompson, 2011; Randel & Wu, 1999; Staehelin et al., 2001; Tarasick et al., 2005; Thompson et al., 2020). The standard balloon launch schedules for long-term stations are most commonly weekly, as appropriate for stratospheric monitoring (Liu et al., 2009), but range from twice monthly to 2–3 times per week.

Strategic ozonesonde networks are used, often with coordinated ground-based, aircraft, and satellite observations, to study ozone processes (Stauffer et al., 2018; Thompson et al., 2007a, 2007b, 2010). The high vertical resolution of ozonesondes is important here, as atmospheric transport occurs in thin, quasihorizontal layers (Newell et al., 1996, 1999). For example, since 1992 the annual Match campaigns (von der Gathen et al., 1995) have followed ozone-depleted layers in the mid- and high-latitude stratosphere as they move in and around the Arctic vortex (e.g., Manney et al., 2011). The INTEX Ozonesonde Network Study (IONS-04 and IONS-06) (Thompson et al., 2007a, 2007b), ARCIONS (Tarasick et al., 2010), BORTAS network study (Parrington et al., 2012) and SEACIONS (http://tropo.gsfc.nasa.gov/seacions) studied episodic influences of stratospheric-tropospheric exchange, convection, and urban and fire pollution in the free troposphere and lower stratosphere over North America.

By linking potential vorticity values denoting stratospheric air to locations of high-ozone/low-H_2O layers in the IONS-04 ozonesonde data, Thompson et al. (2007a, 2007b) determined that ~1/4 of northeastern North American free tropospheric ozone during July to August 2004 originated in the stratosphere. Using ozonesonde data from a series of campaigns at multiple sites, and trajectory modeling, Hocking et al. (2007) and Tarasick et al. (2019a) found that the stratosphere contributed 3.1% of ozone in the boundary layer, 13% in the lower troposphere, and 34% in the middle and upper troposphere. Moeini et al. (2020), combining back trajectories and satellite fire count data with 1,100 ozonesonde profiles at 18 Canadian and northern U.S. sites during the IONS, ARCIONS, and BORTAS campaigns, calculated that up to 8% of tropospheric ozone originated from biomass burning. Cooper et al. (2006) used IONS-04 data and models to determine that the majority of upper tropospheric ozone enhancements over eastern North America were due to lighting NOx production, while Cooper et al. (2010) used trajectories and free tropospheric ozone data to show that emissions in Asia significantly affect ozone pollution in western North America.

The enduring role of ozonesondes in the global observing system owes much to the use of the profile data, from surface to 30 km, in the development of high-quality satellite ozone measurements. Ozonesondes support satellite observations in several important ways.

Ozonesonde profile climatologies (e.g., Fortuin & Kelder, 1998; Lamsal et al., 2004; Logan, 1999; G. Liu et al., 2013a; J. Liu et al., 2013b; McPeters & Labow, 2012) are the basis of retrieval algorithms, including averaging kernels, and are being combined with merged satellite data sets (Hassler et al., 2018; Moeini et al., 2019).

Ozonesondes help validate total ozone and profile retrievals for new satellite instruments. Special observational networks, sometimes part of multiplatform field campaigns, are often organized to collect soundings

for particular satellites shortly after launch. For example, studies published in the Aura Special Issue (Journal of Geophysical Research, 2007) feature the ~700 IONS-06 ozonesondes, timed for the satellite overpass, to evaluate data from the four Aura ozone sensors, including both limb-viewing and nadir instruments. Such campaigns are also conducted at intervals to evaluate the continuing performance of satellite sensors and to check for drift (Walker et al., 2016).

Ozonesonde profiles serve as a transfer standard to allow cross-calibration of multiple satellite instruments. Along with ground-based spectrometers, ozonesonde data are used to compare two or more satellite instruments. The comparisons are often made for a series of instruments of similar design during an overlap period of the operations of a newer instrument with an older one that will be replaced, for example, the SBUV (Fioletov et al., 2006) and GOME series (Hoogen et al., 1999; X. Liu et al., 2005; Miles et al., 2015), IASI (Boynard et al., 2009), the TOMS-to-OMI transition (McPeters et al., 2008; McPeters et al., 2015; Witte et al., 2017), and Meteor to EP TOMS (Antón et al., 2009). The ozonesonde data provide a stable, fixed-site set of reference profiles for different types of satellite instruments, operating on the same or a different platform, to be compared in total column ozone, tropospheric and stratospheric columns, and profiles. Such analyses quantify biases in the satellite profile records, which is important on both shorter and longer-term time scales. This quantification is essential for merging satellite data sets into a long-term record as well as for evaluation of sensor drift.

Ozonesonde data provide important information to evaluate satellite instrument drift. Hubert et al. (2016) did a comprehensive comparison of 14 limb-viewing satellites that have measured lower-mid stratospheric ozone within the past 25 years Hubert et al. (2016) illustrate a newer application of ozonesonde profiles to the limb-viewing satellites that consists of calculating and comparing drift in individual instruments, given that half of those 14 instruments surveyed were operational for a decade or more. The study found discontinuities within a satellite instrument's time series at different levels within the stratosphere. For example, Hubert et al. (2016) found a −15% drift at 18°S (latitude of the Fiji SHADOZ station) to +15% (at Irene) when compared to MLS at 21.5 hPa. The uncertainties in ozonesonde drift at different locations also vary widely. Similar characteristics in ozonesonde-satellite drift comparisons are seen with HALOE data (1991–2005) for which nearly all the ozonesonde comparisons are in the extra-tropics. Hubert et al. (2016) clearly demonstrate that using ozonesonde profiles for satellite drift detection places a requirement on ozonesonde accuracy and precision of 3%–5%.

Lidars and microwave are also used for satellite calibration but there are only a modest number of stations with multidecade records (Hassler et al., 2014; Tarasick et al., 2019b; WMO, 2018).

Ozonesondes also provide a comparative reference for aircraft ozone profiles collected through long-term programs that operate ozone sensors on commercial airliners: for example, MOZAIC-IAGOS and CARIBIC (Petzold et al., 2015; Staufer et al., 2013, 2014; Tarasick et al., 2019b; Thouret et al., 1998).

Figure 1 displays the location of stations for which at least a decade of ozonesonde data is available in open archives, that is, the World Ozone and Ultraviolet Data Centre (WOUDC; woudc.org), the Network for Detection of Atmospheric Composition Change (NDACC; ndacc.org), Southern Hemisphere Additional Ozonesondes (SHADOZ; tropo.gsfc.nasa.gov/shadoz). The majority of these stations also host an operational ground-based total ozone instrument, which can offer a valuable parallel ozone reference.

Ozonesonde-satellite comparisons may also detect biases among ozonesonde profiles measured at various stations, presumably due to differences in ozonesonde instrument type and preparation (Witte et al., 2017, 2018). This was first noted when total ozone measured by tropical ozonesondes at various SHADOZ sites was compared to total ozone from the nadir viewing BUV satellite instruments, TOMS, and OMI (Thompson et al., 2007, 2012). It is known that the performance characteristics of the two ECC types (SPC and EN-SCI) can be significantly different, although this is not yet well understood (Smit et al., 2007). More recently small discontinuities in comparisons between total ozone from ground-based instruments and BUV-type satellites have been found in the progression from OMI to the SNPP/OMPS era (Thompson et al., 2017). Recent changes relative to satellite data observed at a number of stations in the global network (Stauffer et al., 2020) may also be due to changes in sonde response caused by (unknown) manufacturing changes. Changes in sensing solutions, preparation, or other operating procedures can also affect sonde response. This paper reviews the current state of knowledge of ozonesonde uncertainty and bias, based on several
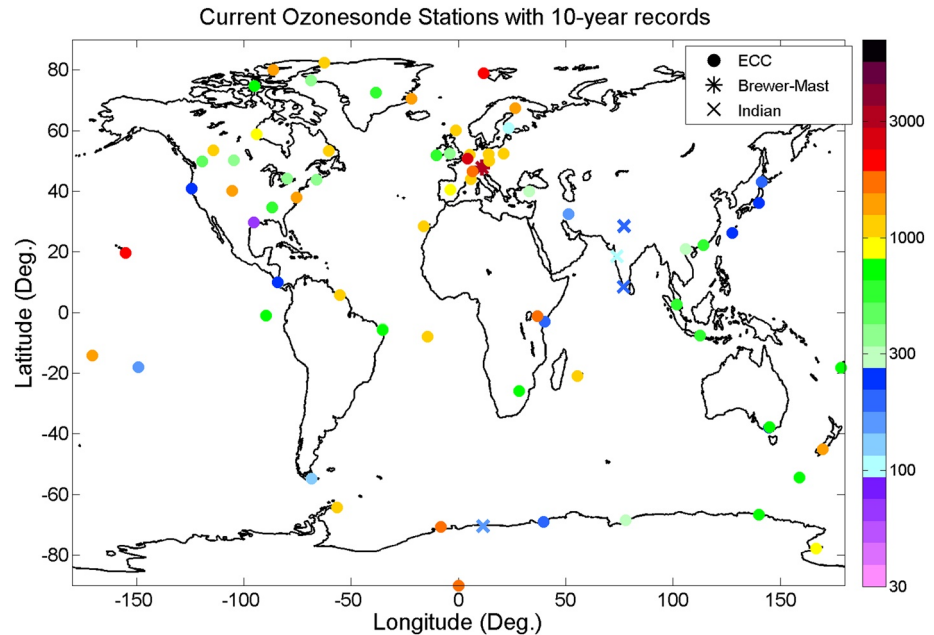
Figure 1. Locations of stations for which at least a decade of ozonesonde data are available in open archives, that is, World Ozone and Ultraviolet Data Centre (woudc.org), Network for Detection of Atmospheric Composition Change (NDACC, ndacc.org), Southern Hemisphere Additional Ozonesondes (SHADOZ, http://tropo.gsfc.nasa.gov/shadoz). The majority of these stations also host an operational total ozone instrument. The color bar indicates the number of profiles of each type available from each station.

recent studies (Deshler et al., 2017; Sterling et al., 2018; Tarasick et al., 2016; Van Malderen et al., 2016; Witte et al., 2018), the ASOPOS report (Smit and ASOPOS Panel, 2014), and the emerging GRUAN protocol (GRUAN, 2019). We also describe sources of error that can be better evaluated with further research, and a "roadmap" for achieving the goal of having all sonde measurements traceable to the modern UV-absorption standard (Hodges et al., 2019; Tarasick et al., 2019b), and better than 5% overall uncertainty throughout the ozone profiles and across the global ozonesonde network.

2. Principles of the Electrochemical Concentration Cell

Ozonesondes are small, lightweight, and compact balloon-borne instruments, developed for measuring the vertical distribution of atmospheric ozone up to an altitude of about 30–35 km. During normal flight operation, ozonesondes are coupled via special interfacing electronics with standard meteorological radiosondes (e.g., Dabberdt et al., 2005) for data transmission of the measured sensor current and aerological parameters like pressure, temperature, relative humidity, and, since the adoption of radiosondes with GPS, drift-based wind direction and wind speed, and GPS-derived altitude. Using the radiosonde telemetry, the current measured by the ozonesonde is transmitted to the ground station for data processing.

Ozonesondes utilize electrochemical detection methods developed originally for surface monitoring (Bowen & Regener, 1951; Brewer & Milford, 1960; Ehmert, 1951; Glückauf et al., 1944; Paneth & Glückauf, 1941; Vassy, 1958). The principle of the ozone measurement is based on the titration of ozone in a neutral-buffered potassium iodide (NBKI) sensing solution according to the redox reaction

$$2\,KI + O_3 + H_2O \rightarrow I_2 + O_2 + 2KOH \tag{R1}$$

followed by

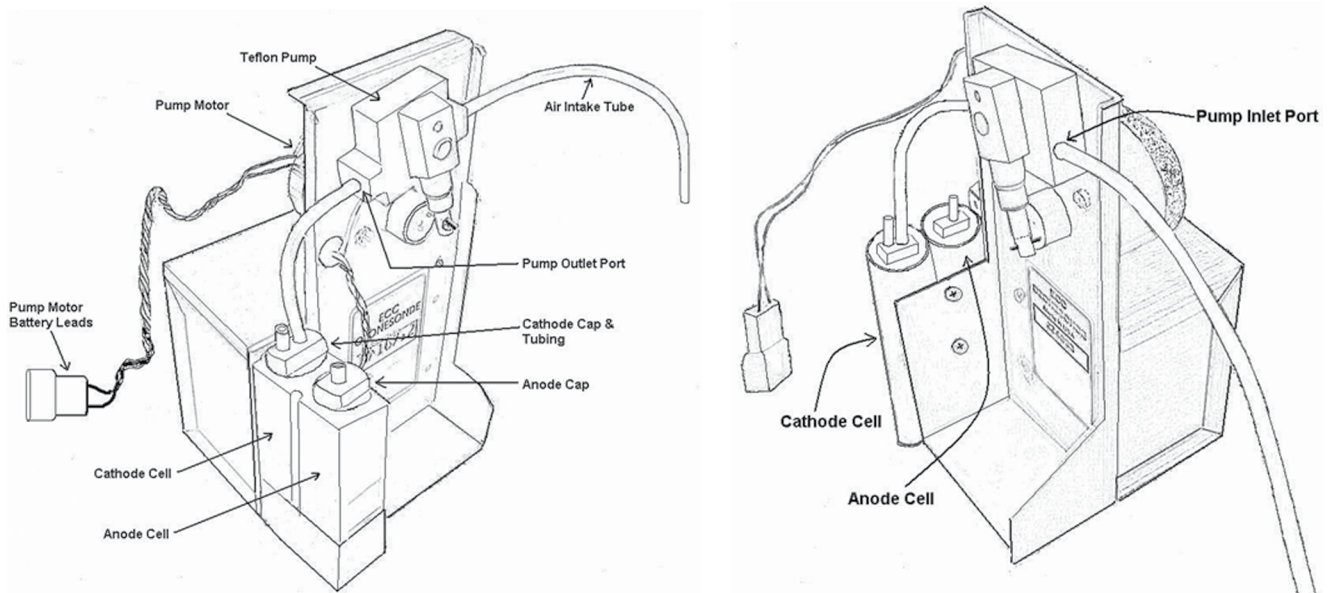$$I_2 + 2e^- \rightarrow 2I^- \tag{R2}$$

Figure 2. Two ECC ozonesonde instruments, made by different manufacturers. Left: SPC-6A type made by Science Pump Corporation; Right: ENSCI-Z type made by ENSCI Corporation. Differences are minor: the cathode and anode caps, thermal contact between the cells and the metal housing, and the plastic used to construct the cells and pump (Teflon and molded plastic, respectively).

The titration is a coulometric method, determining the amount of free iodine (I_2) generated per unit time via conversion to an electric current. The ECC ozonesonde (Komhyr 1969, Figure 2), consists of cathode and anode chambers, each containing a platinum (Pt) mesh electrode, immersed in an aqueous KI-solution, saturated in the anode, and nominally of 1.0% concentration in the cathode (although concentrations from 0.1% to 2% have been used). The two chambers are linked together by an ion bridge (made typically of densely packed cotton fibres) that provides a pathway for the ion chemistry but prevents mixing of the cathode and anode electrolytes. A small gas sampling pump forces ambient air through the cathode chamber sensing solution of the ECC as the ozonesonde ascends. Transported by the stirring action of the air bubbles, the iodine makes contact with the platinum cathode and is reduced back to iodide ions by the uptake of, in the ideal case, two electrons per molecule of iodine as per Reaction R2.

Although other types of ozonesonde instruments have been used in the past (Tarasick et al., 2019b), almost all ozone sounding stations worldwide now use the ECC ozonesonde type, archiving 2,000–3,000 profiles annually. Normally data are taken during a 4–5 m/s ascent to a balloon burst altitude of 30–35 km (12-5 hPa). The inherent response time (1/e) is ∼20–30 s (Smit & Kley, 1998), which corresponds to a vertical resolution of about 80–150 m.

From R1, each O_3 molecule causes (ideally) two electrons to flow in the external circuit. The measured electrical current i_M generated in the external circuit of the electrochemical cell is, after correction for an offset or "background" current i_B, directly related to the uptake rate of ozone in the sensing solution of the cathode chamber. By knowing the gas volume flow rate $\Phi_P = \eta_P \Phi_{P0}$ of the air sampling pump and the air temperature in the pump, T_P, the measured partial pressure of ozone P_{O3} is determined from Faraday's first law of electrolysis and the ideal gas law and is given by the relation:

$$P_{O3} = \frac{\left(i_M - i_B\right)}{\eta_P \eta_A \eta_C} \frac{RT_P}{2F\Phi_{P0}} \tag{1}$$

where R is the universal gas constant and F is Faraday's constant, the constant 2 represents the ideal two electrons from Reaction R2, and

η_P = pump flow efficiency as a function of pressure;

η_A = absorption efficiency to transfer the sampled gaseous ozone into the liquid phase;

η_C = conversion efficiency of the absorbed ozone in the cathode sensing solution into iodine and finally into the measured cell current i_M.

The efficiency of the air sampling pump declines at low pressures in a predictable way, with empirically-derived curves showing some differences between ECC models. The absorption efficiency η_A is usually taken to be 1 (complete absorption). The conversion efficiency is then the number of electron pairs contributed to the measured electrical current i_M by each molecule of ozone, and standard practice is to take $\eta_C = 1$, from Reaction R2.

The use of $\eta_A = 1$ and $\eta_C = 1$ neglects several processes that may affect the number of electrons produced per molecule of ozone: loss of ozone to the sensor walls, less than complete absorption of ozone into the cathode sensing solution, loss of molecular iodine through evaporation from solution (and in rare cases, loss of the solution itself via spraying through the exit tube), losses through the internal resistance of the cell, and reactions other than R1 that can cause the stoichiometry of the NBKI method to be different from 1 (Saltzman & Gilbert, 1959).

Each of these parameters has an associated uncertainty, with both systematic and random components. Here, we define systematic uncertainties as those that do not vary from sounding to sounding, while random uncertainties are those that do vary randomly with each sounding. In general, each of these uncertainty components can be a function of pressure or time. The systematic components, or biases, can be measured or estimated, and so corrected, but the derived corrections will carry their own uncertainties.

Although these uncertainties do not vary randomly within a sounding, a few of these parameters also have a random uncertainty associated with the inflight measurement: T_P, i_M, η_A (due to the stochastic nature of bubble formation), and possibly pump motor speed. From laboratory comparisons using a calibrated ozone source it can be estimated that these total <1%. As they are uncorrelated, they are also reduced by integrating the profile in whole or in part, and so can generally be neglected, except when deconvolving or differentiating the input signal (e.g., De Muer & Malcorps, 1984; Huang et al., 2018; Vömel et al., 2020).

ECC-ozonesondes have gone through several modifications of the instrument and procedures since they were first manufactured in the early 1970s (Johnson et al., 2002; Thompson et al., 2017; Witte et al., 2017, 2018). This includes changes made by the manufacturer (Figure 2), as well as changes in sensing solution (supporting information, Text S4), and to standard operating procedures (Smit and ASOPOS Panel, 2014). These changes, if they introduce new systematic uncertainties in any of the parameters in Equation 1, may cause significant uncertainties in ozonesonde trend analysis (SPARC-IOC-GAW, 1998).

3. Uncertainty Budget Analysis

The instrumental uncertainty of the electrochemical ozone sensor for the measurement of ozone is a composite of the contributions of the individual uncertainties of the different instrument parameters in Equation 1. As these in general depend on the ambient air pressure, the overall uncertainty of the ozone measurement will be a function of pressure, and therefore, altitude.

It is assumed that the uncertainties are random, uncorrelated, and normally distributed, so that the overall relative uncertainty of P_{O3} can be expressed as the combined uncertainties of the variables in Equation 1, plus any additional uncertainties:

$$\frac{\Delta P_{O3}}{P_{O3}} = \sqrt{\left(\frac{\Delta \eta_P}{\eta_P}\right)^2 + \left(\frac{\Delta \eta_A}{\eta_A}\right)^2 + \left(\frac{\Delta \eta_C}{\eta_C}\right)^2 + \frac{\left(\Delta i_M\right)^2 + \left(\Delta i_B\right)^2}{\left(i_M - i_B\right)^2} + \left(\frac{\Delta T_P}{T_P}\right)^2 + \left(\frac{\Delta \Phi_{P0}}{\Phi_{P0}}\right)^2 + \sum \varepsilon_i^2} \qquad (2)$$

Here, the additional term in ε_i represents additional random uncertainties due to other causes: uncertainties associated with any bias corrections applied to the other parameters, and uncertainties in the pressure coordinate or time registration of the ozone signal, which in practice express as uncertainties in ozone partial pressure. For example, an error in pressure, by assigning an ozone value to the wrong pressure altitude, will translate into an effective error in ozone, of magnitude proportional to the ozone gradient.
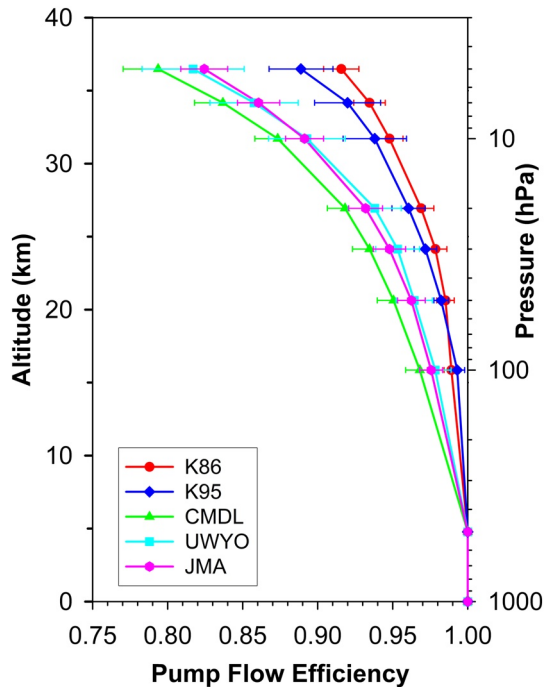
Figure 3. Pump flow efficiencies (η_P) as a function of air pressure for ECC-ozone sondes reported by Komhyr (1986), Komhyr et al. (1995), Johnson et al. (2002): (CMDL and UWYO), and Nakano, personal communication, 2019) (JMA). See also Table S2 in the supporting information.

3.1. Pump Flow Efficiency η_P at Low Pressures

At ambient air pressures <100 hPa the efficiency of the gas sampling pump degrades due to pump leakage, dead volume in the piston of the pump, and the back pressure exerted on the pump by the cell solution (Komhyr, 1967; Steinbrecht et al., 1998), so that the gas volume flow rate measured during preparation Φ_{P0} must be corrected by a factor η_P. This decrease in pump efficiency at reduced pressures is a function of ambient pressure. Because of its importance, a large amount of effort has gone into characterizing the efficiency of ECC pumps at low pressures (e.g., Harder, 1987; Johnson et al., 2002; Komhyr, 1986; Komhyr et al., 1995; Nakano, personal communication, 2019; Torres, 1981). Johnson et al. (2002) summarizes the results of a large number of pump calibrations using complementary methods. More recent measurements are generally consistent within statistical uncertainty, but differ significantly from the Komhyr (1986) and Komhyr et al. (1995) values; we will come back to this in Section 3.3. Measured pump flow efficiencies as a function of ambient pressure for ECC ozonesondes are shown in Figure 3 (see also Table S2), along with measured standard deviations, which may be taken as the uncertainties of the corrections.

While the uncertainty of the pump flow efficiency is modest below 20 km (1.1% at 100 hPa), it increases substantially at pressures below ~20 hPa, and so contributes significantly to the overall uncertainty of the ozonesonde performance above 25–30 km altitude (2%–3% at 10 hPa, and 3%–4% at 5 hPa; Table S2).

3.2. Absorption Efficiency η_A

The absorption efficiency η_A is the capture efficiency (i.e., mass transfer) of the sampled gaseous ozone into the liquid phase of the cathode sensing solution. Although evaporation reduces the amount of cathode solution available for uptake of gaseous ozone, η_A is not significantly affected (e.g., Komhyr, 1971) by the changing liquid volume. At higher altitudes the uptake of gaseous ozone apparently becomes more efficient due to much faster mass transfer (i.e., faster diffusion) at lower pressures (Davies et al., 2003). Thus η_A stays at 1.00, with an uncertainty of less than ±1% throughout the entire profile for ozonesonde sensors charged with 3.0 cm³ of cathode solution. For ECC-sensors charged with 2.5 cm³ of cathode solution (or those that during the day-of-flight calibration procedure are run long enough to evaporate 0.5 ml), only ~96% of the ozone is captured by the sensing solution at 1,000 hPa ground pressure (Davies et al., 2003); at lower pressures the 4% deficit vanishes rapidly such that at pressures below 100 hPa, η_A equals 1.00. For 2.5 cm³ cathode sensing solution at pressures greater than 100 hPa, the absorption efficiency should be calculated as

$$\eta_A\left(P_{Air}\right) = 1.0044 - 4.4 \times 10^{-5} P_{Air} \tag{3}$$

where P_{Air} is in hPa. The uncertainty of η_A is estimated to be ~±0.01 throughout the entire profile, and the additional uncertainty of this correction for ECC-sensors charged with 2.5 cm³ of cathode sensing solution is estimated as ±0.01 (Davies et al., 2003; Smit et al., 2012).

3.3. Conversion Efficiency η_C

The efficiency of conversion of the absorbed ozone into the measured cell current, η_C, includes the stoichiometry of the conversion of iodide into I_2 (R1), as well as several possible loss processes. Losses to the cell walls are likely negligible as the diffusion time constant for the sampled gas in solution is much less than the reaction time constant. Losses of iodine are thought to be small, as most of the iodine in solution is in the form I_3^- (Tarasick et al., 2002). In addition, iodine escaping from solution would also have been detected (as

unabsorbed ozone) in the experiments of Davies et al. (2003) discussed above. Losses to internal resistance (e.g., the conductivity of the ion bridge between the cathode and anode chamber, or of electron transfer at the Pt cathode surface) are not easily quantified, but likely small, as the cell does not show any nonlinearity in its response to ozone.

Based on the limited results of Dietz et al. (1973), Flamm (1977), and Pitts et al. (1976), a random uncertainty of 3% for the stoichiometry of Reaction R1 typically has been assumed (Smit et al., 2012; Sterling et al., 2018; Witte et al., 2018), independent of altitude. This may be an overestimate, as ozonesondes prepared and flown under similar conditions show a precision of 3%–5% throughout most of the profile below ~28 km (Deshler et al., 2008a; Kerr et al., 1994; G. Liu et al., 2009; Smit et al., 2007). On the other hand, the stoichiometry of Reaction R1 increases with time (i.e., altitude) in buffered sensing solutions (Johnson et al., 2002); the uncertainty of the stoichiometry may increase with altitude as well. In addition, loss of water through evaporation during flight will concentrate both the KI and the buffer, and both effects will increase the stoichiometry of R1.

The stoichiometry of Reaction R1 has been studied extensively since its discovery in the 19th century. Many early studies were made for ozone concentrations much higher than those in the stratosphere, because of the difficulty of working with low concentrations of ozone at the time (A. W. Boyd et al., 1970; Dietz et al., 1973; Hodgeson et al., 1971; Kopczynski & Bufalini, 1971). Byers and Saltzman (1959) and Saltzman and Gilbert (1959) found that the reaction stoichiometry varied with pH, being 1.00 at pH = 7, and in general much lower at higher pH values and in unbuffered solution. Without buffering, Reaction R1 will drive the solution alkaline, so the KI solution is normally buffered. Dietz et al. (1973) found a stoichiometry of 1.00 ± 0.03 at pH = 7 for two measurements at 100 and 400 ppbv of ozone. Flamm (1977) found a value of 1.2 for ozone mixing ratios between 350 and 1,000 ppbv, noting that it increased with time, and 0.962 ± 0.07 for a mixing ratio of 100 ppbv. Pitts et al. (1976) found the 2% NBKI method gave (a) NBKI/IR = NBKI/UV = 1.23 ± 0.06 for RH = 50% at 100–1,000 ppb of ozone and (b) NBKI/IR = NBKI/UV = 1.14 ± 0.04 at RH = 3%. Although they had no explanation of the apparent water vapor dependence, they found it was reduced when potassium bromide was added (Bergshoeff et al., 1980; Lanting, 1979), as is commonly the case in ozonesondes. However, Johnson et al. (2002) found that KBr concentration had no significant influence on ECC sonde response, so the role of KBr in ozonesondes is an unresolved question.

Saltzman and Gilbert (1959) note that the differences in stoichiometry found at different pH values imply that the chemistry of reaction of ozone with KI is complex, involving reactions other than R1 that cause loss of iodine, as well as reactions that produce additional iodine. Several authors have noted the existence of slow side reactions involving the phosphate buffer, with a time constant of about 20 min, that may also change (increase) the stoichiometry from 1.0. The measured magnitudes vary, from about 11% (Saltzman & Gilbert, 1959), to as much as 15%–30% (Flamm, 1977) in glass laboratory impingers; in ECC sondes 10%–15% (Johnson et al., 2002), and Brewer-Mast sondes 4%–6% (Tarasick et al., 2002).

Some of the differences in the laboratory results of the 1970s may in fact be due to differences in the length of time for the measurement, which would affect the stoichiometry through these side reactions with the buffer. Several authors (e.g., Flamm, 1977; Saltzman & Gilbert, 1959) note apparent differences in performance resulting from laboratory dust, or use of different brands or grades of solution chemicals and distilled versus de-ionized water, suggesting that these differences could be due to trace contaminants. Such an issue could conceivably affect ozonesonde performance as well.

Evaporation causes the concentration of the sensing solution to increase, which can further enhance the stoichiometry of the NBKI reaction, by concentrating the phosphate buffer, and to a lesser degree, by increasing the concentration of the KI itself (Johnson et al., 2002). This enhancement of the sensitivity of the ECC sensor will also increase the uncertainty of the measured ozone, introducing a systematic uncertainty that can increase significantly with altitude (e.g., I. Boyd et al., 1998; Johnson et al., 2002; Smit et al., 2007).

Given the uncertainty in the precise chemistry occurring in the cell, it is difficult to estimate the uncertainty in its stoichiometry. Nevertheless, most recent comparisons to UV photometry in the laboratory environmental chambers or in balloon-based intercomparisons find ratios close to 1.0, and ECC sondes give results that agree very well with coincident total ozone measurements. This is because the pump flow efficiencies used in past practice (Komhyr, 1986; Komhyr et al., 1995) in fact represent an overall correction that
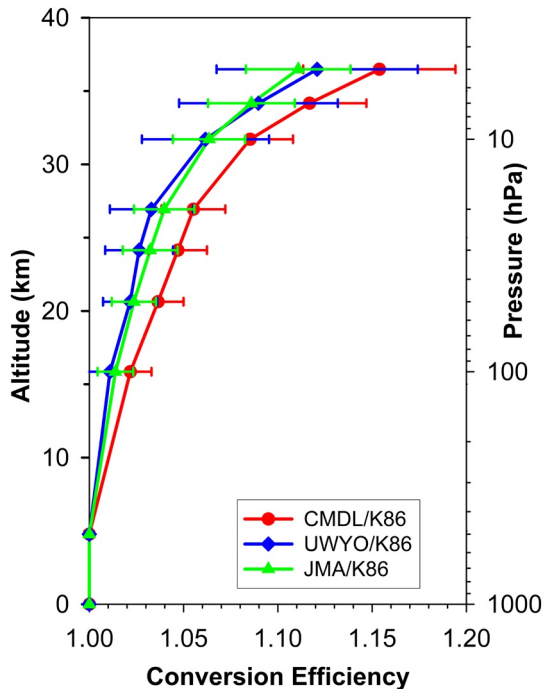
Figure 4. Estimated change in stoichiometry during a typical ozonesonde flight, derived from the pump correction differences in Figure 3.

includes both the pump flow efficiency as well as an estimate of the increase in stoichiometry over the duration of a flight (Sterling et al., 2018; Witte et al., 2018). Figure 4 makes this clear: it shows the ratio between the Komhyr (1986) pump flow efficiencies and the more recent, accurate determinations. These ratio curves show an increase with altitude that mimics the expected increase in stoichiometry with time and ozone exposure discussed above, and they agree well with the experimental results of Johnson et al. (2002), who found that the stoichiometry of R1 over a 2-h period (a typical time of flight for an ozone sounding) increased from 1.00 to 1.05–1.20, with the overall increase depending mainly on the concentration of the phosphate buffer and to a minor degree on the KI concentration.

That is, the low Komhyr "pump corrections" are compensating for the increase in stoichiometry during a flight due to the slow side reactions. They do this quite well, since ECC sondes have average total ozone normalization factors close to 1.00. However, this will be true only on average, as the actual pump flow efficiency is a function of pressure, and the increase in stoichiometry is a function of ozone exposure and time.

While the curves in Figure 4 may approximate average values for conversion efficiency, actual values will vary with sensor construction and KI solution type. The JOSIE (Juelich Ozone Sonde Intercomparison Experiment) experiments at the World Calibration Centre for Ozone Sondes (WCCOS; see supporting information, Text S1) demonstrated that the performance characteristics of the two ECC types (SPC and ENSCI) can be significantly different, although operated under the same conditions (Smit et al., 2007). The biases are reasonably consistent and so can be removed by the transfer function suggested by Deshler et al., (2017), with an additional uncertainty in Equation 2 of ±5%. The reasons for these differences are not well understood, but they demonstrate that the conversion efficiency (η_C) is different for apparently modest differences in sonde construction, and so may be different for other changes in manufacture or in preparation. Recent changes relative to satellite data observed at a number of stations in the global network (Stauffer et al., 2020) may also be due to changes in η_C caused by manufacturing changes.

The JOSIE experiments also describe significant differences in the ozone readings when ECC-ozonesondes of the same type are operated with different cathode solution strengths (Text S4; Table S4). For both ECC types, the use of 1.0% KI and full buffer gives 5% larger ozone values compared with the use of 0.5% KI and half buffer, and as much as 10% larger values compared with 2.0% KI and no buffer (Smit et al., 2007). The recent JOSIE-2017 (Thompson et al., 2019) revisited the issue of instrument-sensing solution composition combinations for tropical simulations that mimicked the conditions prevalent at SHADOZ stations. The biases observed in JOSIE-2000 and BESOS were confirmed. Ozone profiles based on a new variant (SST0.1 in Table S4) were compared to those from sondes prepared with the standard solutions (Smit & ASOPOS, 2014). The SST0.1 variant reduced errors in the tropopause region, where ozone values are very low in tropical situations, but total column ozone tended to be biased low relative to the standard cases and to the JOSIE reference photometer (Thompson et al., 2019).

An indirect estimate of the uncertainty of η_C and its increase with altitude can be obtained from the pump flow efficiency uncertainties and the standard deviations of total ozone normalization factors. However, a comprehensive analysis of results from JOSIE can give a more direct evaluation of the stoichiometry in the cell, as well as its variation with flight time. It should be straightforward to develop, from existing data, new empirical correction functions that will look something like the curves in Figure 4, and represent the variation and uncertainty of η_C with respect to altitude, each sensor model, and preparation (Smit et al., in preparation).

In the following section, we present an alternative way of treating the stoichiometry variation, and show that to a large degree the slow response due to the slow side reactions can be treated as a time-varying "background current."
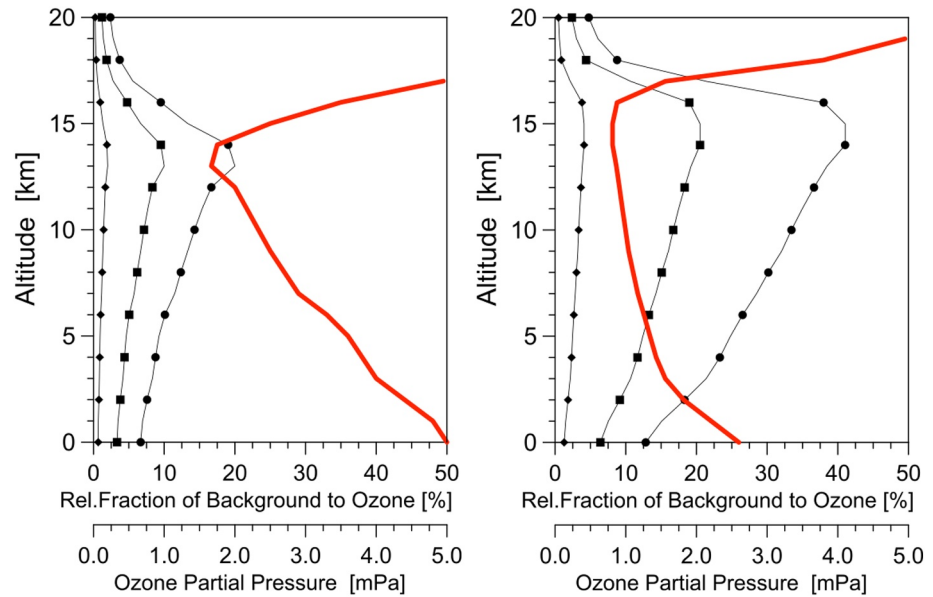
Figure 5. Contribution of the background current of the ECC-ozone sensor as a relative fraction of the vertical profile of ozone (solid red line i_M (mPa)) for background values of 0.01μA (◆), 0.05μA (■), and 0.1μA (●) at mid-latitudes (left) and in the tropics (right).

3.4. Measured Cell Current i_M and Background Current i_B

The uncertainty of the measured sensor current (i_M) is mainly determined by the accuracy of the current measurement by the electronics (current (i) to voltage (V) converter) of the ozonesonde data interface board, such that for currents > 1.0 μA the uncertainty of i_M is about ±1%, while for currents < 1 μA the uncertainty will be about ±0.01 μA (Smit & ASOPOS Panel, 2014). Sterling et al. (2018) present a more detailed analysis of the measurement precision of several interface boards.

Prior to the balloon launch the response of each ozonesonde to ozone-free air is individually determined at several points in the preparation process. i_B0 is measured after charging the cells but before the introduction of ozone. i_B1 is measured after exposure of the cathode cell to 10 min of ozone of concentration that produces a current of 5.0 μA followed by sampling of zero air (or air from the "No/Lo" ozone port of the ozonizer unit) for 10 min. (Formerly, the recommendation was "until the current stabilizes" [Smit & ASOPOS, 2014], but the point at which it stabilizes is somewhat subjective, as in general the current continues to decline slowly with time [Vömel and Diaz, 2010].) i_B2 is measured at the launch site sampling zero air or ambient air passing through an ozone filter. One of these values is generally treated as a constant offset and subtracted from the measured cell current (Equation 1).

Background signals at the surface typically correspond to 0.1–0.5 mPa ozone. Ozone soundings are thus sensitive to the background signal correction in regions where the ozone concentrations are low, for example, the tropical upper troposphere (Kley et al., 1996; Newton et al., 2016; Vömel & Diaz, 2010) and the winter/spring polar stratosphere during the season of ozone depletion (Vömel & Diaz, 2010).

Figure 5 shows the ratio of the background current to the measured ozone current for ozone profiles that are typically encountered at midlatitudes (left) and in the tropics (right).

Modern ozonesondes report "final background" currents (i_B2) of 0.03–0.11 μA. This may depend on the quality of the filter used and the time since exposure to ozone. Quantifying the uncertainty of the background current has remained difficult due to our poor understanding of its origins. Sterling et al. (2018) estimate an average for i_B2 of ±0.02 μA for well-prepared sensors, while Witte et al. (2018), for a tropical network, find ±0.02 μA for Science Pump Corp. (SPC) sondes and ±0.03 μA for ENSCI sondes. From Figure 5, it is evident that the uncertainty in the background current dominates the uncertainty of the ozone measurement in the troposphere, particularly in the tropics and the tropopause transition region.

Table 1
Survey of Average Background Current (±1σ) Before (i_B0), and Following Exposure to 150–200 ppbv Ozone (i_B1), During Preflight Preparations of ECC-ozonesondes During JOSIE and BESOS Campaigns (Deshler et al., 2008; Smit et al., 2007)

ECC sonde type		ENSCI-Z		SPC-6A	
Study	SST	i_B0 [μA]	i_B1 [μA]	i_B0 [μA]	i_B1 [μA]
JOSIE1996	SST1.0	0.05 ± 0.01	0.07 ± 0.02	0.02 ± 0.01	0.07 ± 0.01
JOSIE1998	SST1.0	0.05 ± 0.02	0.11 ± 0.03	0.03 ± 0.02	0.11 ± 0.01
JOSIE2000	SST1.0	0.02 ± 0.03	0.06 ± 0.05	0.02 ± 0.01	0.05 ± 0.02
JOSIE2000	SST0.5	0.02 ± 0.02	0.05 ± 0.02	0.00 ± 0.01	0.03 ± 0.02
JOSIE2000	SST2.0	0.02 ± 0.02	0.06 ± 0.03	0.02 ± 0.01	0.05 ± 0.03
BESOS2004	SST1.0	0.00–0.02	0.05–0.06	0.00–0.01	0.04–0.07
BESOS2004	SST0.5	0.00–0.01	0.02–0.03	−0.02–0.02	0.01–0.02
JOSIE2009	SST1.0	0.02 ± 0.01	0.05 ± 0.01	0.01 ± 0.01	0.04 ± 0.01
JOSIE2009	SST0.5	0.02 ± 0.01	0.04 ± 0.01	0.01 ± 0.01	0.03 ± 0.01
JOSIE2010	SST1.0	0.02 ± 0.01	0.04 ± 0.02	0.00 ± 0.02	0.04 ± 0.01
JOSIE2010	SST0.5	0.01 ± 0.01	0.02 ± 0.01	0.00 ± 0.03	0.03 ± 0.01

Note. In all cases, the sensor was flushed for 10 min with ozone-free air before the background current was measured. Sensing solution types (SST) are given in Table S4. See supporting information, Text S4.

The nature of the background current in ECC sondes has been a subject of concern since the introduction of the ECC sonde in the 1970s. ECC ozonesondes exposed to ozone-free air were observed to produce a small current which varied between sondes and with their preparation. The concept was apparently introduced by Komhyr (1969), who suggested that it was due to reaction with oxygen. Laboratory studies (Smit et al., 1994; Thornton & Niazy, 1982, 1983) indicate, however, that the background current in the ECC ozonesonde shows no oxygen dependence. While other oxidants such as NO_2 and H_2O_2 can produce iodine via Reaction 1, the response is small, for NO_2 about 5%–10% of that for ozone (Pitts et al., 1976; Tarasick et al., 2000; Volz & Kley 1988), so the result will be ~0.01–0.03 μA at typical background concentrations of NO_2 (4–12 ppbv).

A cell in equilibrium will produce no current; any current in the absence of ozone or other oxidants must be due to an imbalance of tri-iodide between the anode and cathode cells. Possible causes of such an imbalance include (1) a leaky ion bridge, (2) residual tri-iodide when the ozonesonde is freshly charged with sensing solution (Thornton & Niazy, 1982), (3) an imbalance resulting from cell conditioning or contamination, or (4) previous exposure to ozone. Only the first case represents a background current that may be expected to remain roughly constant and should therefore be subtracted as a best approximation; the others should decline according to the response time of the cell.

Table 1 shows average background currents before (i_B0), and after exposure to 150–200 ppbv ozone (i_B1), obtained during preflight preparations of ECC ozonesondes during several laboratory and field campaigns. Although the background currents of the SPC-6A and ENSCI-Z ozonesondes are of the same magnitude, they both are significantly larger after exposure to ozone. This enhancement effect of the background current, from values of 0.00–0.05 μA before ozone exposure to 0.03–0.11 μA after exposure to ozone, is the result of a minor but still slowly decaying contribution to the measured cell current. By waiting a longer period of time after exposure to ozone, the background currents will drop into the range originally measured (i.e., i_B1 converges with i_B0 over time). From the preceding discussion, it is clear that this is due to the fact that the NBKI chemistry has both a dominant fast and additional minor slow reaction pathway, the latter due to slow side reactions in the cathode sensing solution (Johnson et al., 2002; Saltzman & Gilbert, 1959; Tarasick et al., 2002), and possibly other slow processes such as the mass transport rate in the cell (Thornton & Niazy, 1982, 1983). The magnitude of the slow reaction, however, is strongly related to the concentration of the phosphate buffer in the cathode sensing solution (Johnson et al., 2002; Saltzman & Gilbert, 1959; Vömel & Diaz, 2010; Witte et al., 2019). A large component of the background current is therefore an integral
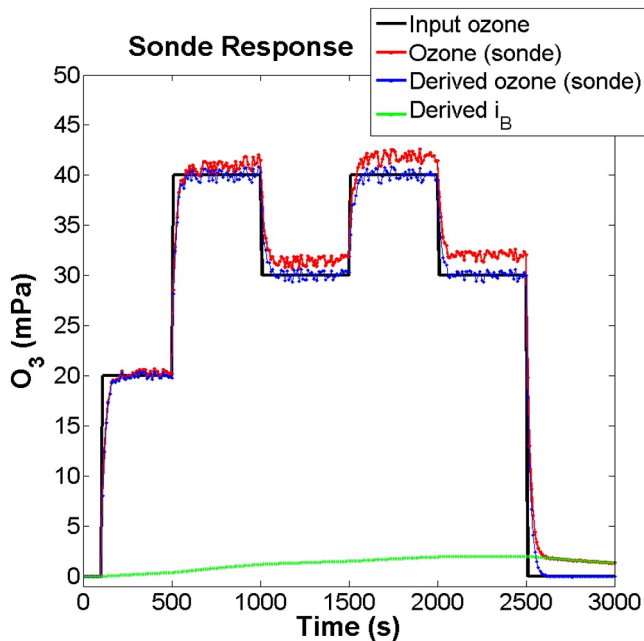
Figure 6. Modeled response of the ECC-ozone sensor (red) to a changing input of ozone (black), for $\tau = 20$ s and $\zeta = 20$ min. The blue curve is the derived ozone after subtraction of the green curve, the calculated slow response (background current).

of previous exposure to ozone and will be different at each point of the profile, with no relation to its value at the ground. One way to deal with this is through deconvolution of the measured signal and the response function of the combined sensor and air sampling system (De Muer & Malcorps, 1984; Huang et al., 2018). Such methods are sensitive to noise in the input signal, and deconvolution of ECC ozonesonde profiles has not been standard practice. New approaches (Vömel et al., 2020) show great promise.

In the laboratory it is observed that sonde response to a constant ozone input is composed of a fast and a slow component, each of which asymptotically with time approaches a constant value with respect to the ozone input. For the fast response this ratio is ~1, while for the slow response a range of estimates exists (Section 3.3). If we consider that the sonde output is the integral over time of its exposure to ozone, of two different processes, the change in response to an amount of ozone over a time interval Δt can be modeled as the sum of

$$\Delta O_3^{\text{fast}}\left(\Delta t\right) = \left(O_3^{\text{true}} - O_3^{\text{fast}}\right)\left(1 - e^{-\Delta t/\tau}\right) \tag{4}$$

and

$$\Delta O_3^{\text{slow}}\left(\Delta t\right) = 0.07\left(O_3^{\text{true}} - O_3^{\text{slow}}\right)\left(1 - e^{-\Delta t/\zeta}\right) \tag{5}$$

where τ is the primary response time constant (~20 s) and ζ is the secondary response time constant (~20 min). The empirical value 0.07 for the magnitude of the slow response is taken from Johnson et al. (2002).

Figure 6 shows the modeled response of the ECC-ozone sensor to a changing input of ozone (O_3^{true} in Equations 4 and 5). The red curve, O_3^{sonde}, is the total of the fast and slow components, summed up to time t. An additional component of random noise has been added. The magnitude of this noise component is taken from laboratory data for similar experiments with an ECC sonde connected to a calibrated ozone source.

In the absence of noise, Equation 4 can be used to retrieve the input ozone, O_3^{true}, from the output signal (differencing and dividing by the time response, and subtracting the slow component). However, with a typical amount of noise the differencing produces a result that is several times noisier than the red curve.

The slow component can be calculated from Equation 5 by assuming as a first guess

$$O_3^{\text{true}}\left(t\right) \approx O_3^{\text{sonde}}\left(t\right) \tag{6}$$

Subtracting the calculated slow component produces a better estimate for O_3^{true}, and Equation 5 can be applied again. This converges in two iterations to produce the green curve in Figure 6. The blue curve is the derived ozone, after subtraction of the green curve from the sonde output. The first-order response of Equation 4 has not been corrected, but the slow response has been removed. This does not add appreciable noise as this component of the signal is slowly varying.

It is clear that the slow response represented by the green curve can explain the observed increase with time of the sonde response to a constant ozone input and also for the slow decay of that response when the ozone input goes to zero. It therefore describes the behavior of the time-varying component of the background current discussed above.

Figure 7 shows the same simple model applied to an ECC sonde profile from the JOSIE1996 WCCOS chamber experiment. The gray curve is the percentage contribution of the slow response (Equation 5), and can be considered an increase in stoichiometry or conversion efficiency. It is generally similar in shape to Figure 4, and even more similar to the experimentally obtained curves of Johnson et al. (2002; their Figure 2).
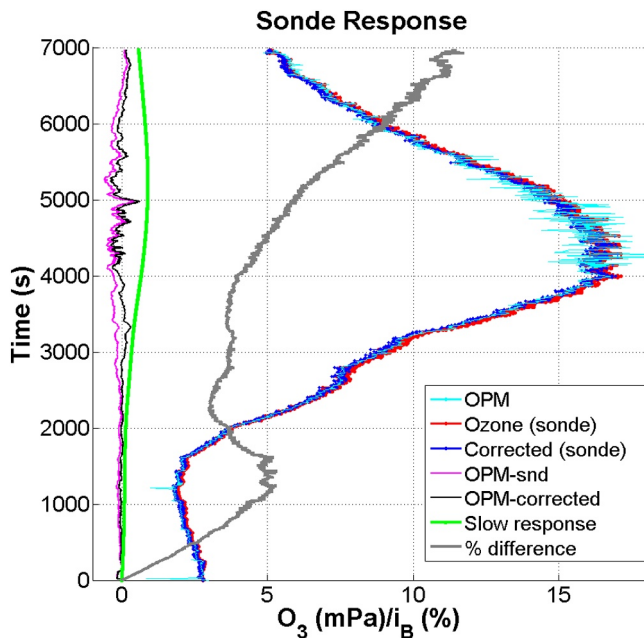
Figure 7. Response of an ECC-ozone sensor in JOSIE1996. The red curve is the original sonde profile with standard corrections for background current and pump efficiency (Komhyr, 1986). The blue curve is the derived profile after subtraction of the green curve, the calculated slow response, and using the CMDL pump efficiency corrections of Figure 3. The agreement with the chamber ozone photometer (OPM) is significantly improved (pink and black curves), with changes of as much as 1 mPa in the regions of strong gradients. The gray curve is the ratio of the slow response to the total response. It is more than 5% of the total response at all points in the profile except in the lower troposphere. Assumed $\tau = 20$ s and $\zeta = 20$ min.

Equivalently, it can be considered an error due to a time-varying component of the background current, and simply subtracted. The result (the blue curve in Figure 7) assumes a conversion efficiency (stoichiometry) of 1 (Equation 4). Here, we have used the CMDL pump efficiency corrections (Figure 3). In this case the agreement with the chamber ozone photometer indeed improved, with changes of as much as 1 mPa in the regions of strong gradients: differences are reduced almost everywhere in the profile, and the sonde integrated ozone is reduced from 350.7 to 344.3 DU, in close agreement with the photometer at 344.5 DU. This excellent agreement may be in part fortuitous; as noted in Section 3.3, conversion efficiency, as well as the magnitude of the slow response, will certainly vary with ECC sonde type and KI solution, and likely with altitude as well. For example, the SPC and ENSCI sonde types show different rates of solution loss in flight, and this may cause differences in conversion efficiency that vary with altitude in a different way from the time- and ozone-dependent background current.

These initial results present a promising avenue for improving the treatment of the background current in ozonesondes, but they need to be tested, using existing JOSIE data, to show how well they in fact model the behavior of the background current, and to what extent the constant terms in Equations 4 and 5 vary under flight (chamber) conditions, and/or from sonde-to-sonde. We anticipate that this new procedure will produce a more accurate result in general. Vömel et al. (2020) have shown much better results in the tropical tropopause region. Another possible effect would be to raise ozone estimates above 30 km (where the differences in Figure 3 are largest), which would reduce some of the larger biases with respect to satellite measurements (Hubert et al., 2016; see their Figure 8).

3.5. Pump Temperature T_P

The air mass flow rate through the sensor is dependent on the air temperature (Equation 1), which is measured in-flight either inside the pump or in the instrument enclosure (polystyrene foam box). Over the course of a sounding the pump temperature can decline by 10–25 K. Since 1996, both ECC ozonesonde manufacturers provide a hole drilled into the Teflon block of the pump. This allows a measurement of the "internal pump temperature" with an estimated uncertainty of about 0.5 K. However, measurements made in the simulation chamber at WCCOS have shown that the pump piston temperature is about 1–3 K higher (increasing linearly with decreasing log pressure) than the measured internal pump base temperature (Smit et al., 2012). Since the sampled air temperature is most closely approximated by the pump piston temperature, the internal pump base temperature must be corrected by this temperature difference as a function of ambient air pressure (in hPa) by:

$$T_{p,\text{piston}} - T_{p,\text{Int}} = 3.90 - 0.80 Log_{10}\left(P_{\text{Air}}\right) \text{ at } P_{\text{Air}} > 3\,\text{hPa} \qquad (7)$$

The 1σ uncertainty of this regression fit is about ±0.5 K. We therefore recommend an uncertainty of ±0.5 K for this correction.

As the outside air is generally much colder than the pump, the thermalization efficiency of the inlet tube to equalize the temperature of the sampled air from ambient to pump conditions must also be considered. Theoretical and experimental analysis has shown that this is very rapid, and thermalization efficiency is 1 with uncertainty smaller than ±0.5%. (Smit, personal communication).
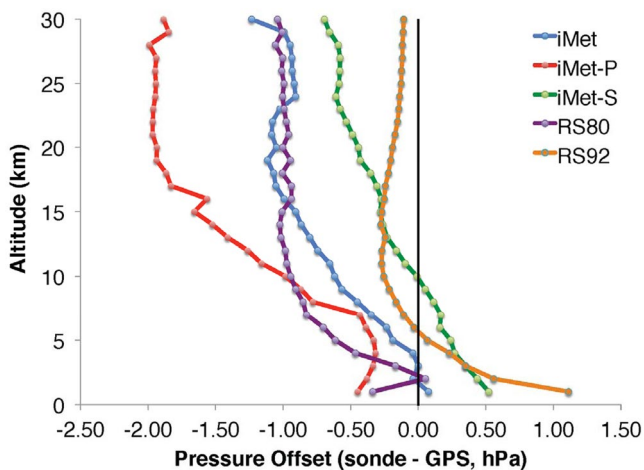

Figure 8. Mean pressure offset data from Stauffer et al. (2014).

The estimated uncertainty of the thermistor measurement itself is ±0.5 K for modern sonde interfaces, while for older interfaces with rod-type thermistors it is estimated as ±1.0 K. In either case the sum of these uncertainties is about 0.3%.

Before 1996 the pump temperature was approximated via a thermistor measurement either in the sensor box or taped or glued to the pump base. Corrections for the differences between these measurements and the pump temperature have been developed (Smit et al., 2012; see also supporting information, Text S2) following chamber and field experiments (Kivi et al., 2007; Komhyr & Harris, 1971; O'Connor et al., 1998; Smit et al., 2007). The additional uncertainty of these corrections is estimated as ±0.5 K for the thermistor glued to the pump base, and for the other methods a pressure-dependent uncertainty of about ±2 K (Text S2). If the pump temperature was measured but not recorded in the processed data file, corrections may be made by using the ratio of the corrected temperature to the measured temperature; in this case a very small additional uncertainty is introduced, equal to ±0.5 K times the relative uncertainty in the actual pump temperature (Tarasick et al., 2016).

In some early (1970s) sounding systems the pump temperature may not have been measured, and an estimated (or constant) pump temperature applied. This can introduce errors, typically of 10–15 K (3%–5%), which imply additional (1σ) uncertainties of ±3% in the calculated ozone, with the largest uncertainties at higher altitudes (SPARC-OTA-GAW, 1998). For reasonable assumptions about the time evolution of the sonde box temperature this can be smaller: Witte et al. (2017) calculated a 3°C–4.5°C standard deviation throughout the profile when constructing a pump temperature climatology from radiosonde (Vaisala RS80) measurements.

3.6. Pump Flow Rate Φ_{P0} at the Ground

The volumetric flow of the gas sampling pump of each ozonesonde at the ground before flight (Φ_{PM}), is individually determined using a bubble flow meter at the gas outlet of the sensing cell. The uncertainty $\Delta\Phi_{PM}$ of this measurement can be estimated from the standard deviations of recorded values for this measurement, of 0.1%–0.3% (Tarasick et al., 2016). For the automated version of this with a commercial flow calibrator, standard deviations are about half as large, but drift can occur if the instruments are not cleaned regularly. Differences between this measurement and the manufacturer's flow rate determination are larger, with standard deviations of about 1%, suggesting operator-dependent biases, or pump motor speed variations of this magnitude. A conservative estimate of $\Delta\Phi_{PM}$ for moist air is therefore ±1%.

Pump motor speed variations have been thought to be negligible in the past, but there are indications that this may be an additional source of uncertainty with newer sondes (B. J. Johnson, private communication).

In addition, the sampled air, typically nonsaturated, or even dry, is forced through the sensing solution before entering the bubble flow meter. Evaporation of water in the sensing solution or in the bubble flowmeter adds to the volume of the air forced through the pump. Therefore, the measured pump flow rate (Φ_{PM}) has to be corrected for this "moistening effect" (Smit & ASOPOS Panel, 2014; Text S3) to yield the actual pump flow rate (Φ_{P0}):

$$\Phi_{P0} = \Phi_{PM} \bullet \left[1 - \left[1 - \frac{RH_{Lab}}{100} \right] \bullet \frac{P_{H_2OSat}(T_{Lab})}{P_{Lab}} \right] \tag{8}$$

where P_{Lab} and T_{Lab} are the air pressure (hPa) and temperature (K) in the laboratory, RH_{Lab} is the relative humidity of the sampled air at the intake of the pump (%), and $P_{H2O,Sat}(T_{Lab})$ is the saturated water vapor pressure in hPa at T_{Lab} (see Table S1). In very dry conditions this error can be as large as 3.3% (P_{Lab} = 960 hPa; T_{Lab} = 25 C).

If measurements of RH_{Air}, P_{Lab}, and T_{Lab} are available then this correction can be made with negligible uncertainty. However, if these are unavailable the uncertainty of this correction depends on the uncertainty of the estimates of these quantities, primarily RH_{Air} and T_{Lab}. For typical variations of RH_{Air} and T_{Lab} found in indoor environments, the additional uncertainty due to this correction is likely between 0.5% and 1%.

As noted above, the pump piston temperature, which most closely approximates the sampled air temperature, is about 2 K larger than the internal pump base temperature, or T_{Lab} in this case. This implies that Φ_{PM} should be corrected by a factor

$$\frac{T_{\text{pump}} - T_{\text{Lap}}}{T_{\text{Lap}}} \tag{9}$$

with an additional uncertainty of ±0.5 K.

3.7. Time Response

The finite first-order response time of ECC sondes (the "fast" component of Equation 4) causes the measured ozone to lag changes in the ozone concentration as the balloon rises. This lag results in modest biases that can in principle be removed (e.g. Huang et al., 2018; Vömel et al., 2020), but this is not currently standard practice. Average biases can be easily estimated, but do not affect trends as the response time of sondes has not changed.

In the absence of correction for the response lag, different balloon ascent rates will give somewhat differing ozone amounts, especially in parts of the atmosphere with large ozone gradients. This difference is proportional to $e^{-\Delta t/\tau} \nabla_t \text{O}_3$, where Δt is the time interval between successive measurements, τ is the e^{-1} response time, and $\nabla_t \text{O}_3$ is the vertical gradient of ozone with respect to time, $\frac{\Delta \text{O}_3}{\Delta t}$ or $w \frac{d\text{O}_3}{dz}$, where w is the rise rate. The random uncertainty due to response time is then proportional to the random uncertainty in balloon rise rate:

$$\varepsilon_{LT} = \frac{1}{\text{O}_3} \frac{\Delta w}{w} e^{-\Delta t/\tau} \nabla_t \text{O}_3 \Delta t \tag{10}$$

The typical variation of balloon rise rates adds very modest uncertainty (<1%) at the sharp ozone gradients near the tropopause and mostly insignificant uncertainty elsewhere (Tarasick et al., 2016).

3.8. Impact of Radiosonde Pressure Measurements on Ozone Sounding Profile

Pressure offsets appear frequently in data from radiosondes that use an on board pressure sensor. These offsets impact ozone profiles in two ways: first, they shift the profile in altitude, displacing the ozone peak vertically, and second, they change the ozone mixing ratio as computed from the ozone partial pressure and the ambient pressure. The magnitude of the resulting errors is comparable to if not greater than other instrumental uncertainties, making identification of pressure offset errors a critical element in processing of ozonesonde data, identification of the error budget, and minimization of the overall uncertainty in the reported ozone profiles.

The impacts of the pressure offset errors on the ozone profile shape also necessarily impact the total column ozone computed from the ozonesonde profiles, introducing biases and uncertainties into comparisons with ground-based and satellite total column ozone instruments.

Inai et al. (2015) examined 30 tropical ozonesonde profiles from the Soundings of Ozone and Water in the Equatorial Region (SOWER) gathered December 2003 to January 2010. Their payloads included the Vaisala RS-80 radiosonde with an onboard GPS unit. They found a mean pressure bias of −0.4 ± 0.2 hPa between 20 and 30 km as determined through intercomparisons of pressure altitude and GPS data.

Steinbrecht et al. (2008), examining 109 twin flights of Vaisala RS-80 and RS-92 radiosondes at two sites in Germany, found typical pressure biases for the RS-80 of about −0.2 to −0.5 hPa in the stratosphere, and negligible biases for the RS-92, but systematic differences for some batches of RS-92 sondes of as much as 0.4 hPa. Precision of the RS-92 pressure sensor was almost an order of magnitude better, at 0.1 hPa.
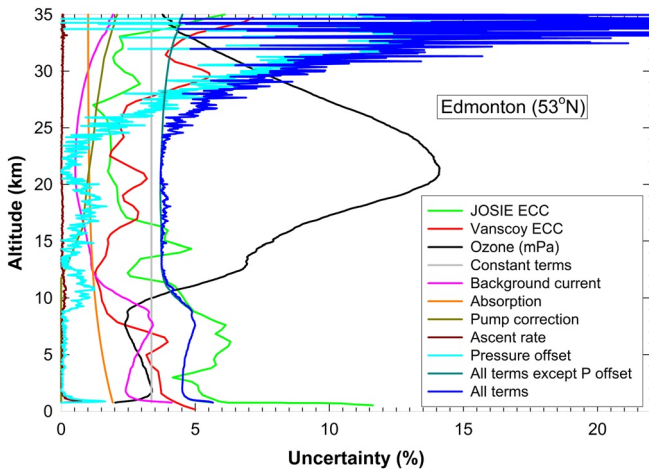
Figure 9. Uncertainty analysis for a northern midlatitude station (Edmonton, Canada), showing the influence of different uncertainty terms, for the assumed values in Table 2. For older sondes without GPS altitude registration, the uncertainty due to pressure bias dominates at higher altitudes. Also shown for reference are profiles of the standard deviation of differences from the midlatitude reference profile during the JOSIE 1996 intercomparison (Smit et al., 2007) and the Vanscoy 1991 intercomparison (Kerr et al., 1994).

Nash et al. (2006) and da Silveira et al. (2006), in two WMO intercomparison of radiosonde systems, find maximum average pressure biases between about 0.5 and 1 hPa, with RMS errors up to 3 hPa.

Stauffer et al. (2014) examined 731 ozonesonde profiles taken from 2005 to 2013 over a wide range of latitudes and using several models from two leading radiosonde manufacturers. Figure 1 in Stauffer et al. (2014) demonstrates the characteristic shape of the pressure and altitude offsets as determined through comparisons of GPS (or GPS-derived) and pressure sensor derived (or pressure sensor) altitude (or pressure) data. Stauffer et al. (2014) found that more than half of the instruments recorded pressure offset magnitudes > 0.6 hPa and nearly one third > 1.0 hPa by the time the radiosonde had reached 26 km. The largest mean pressure offsets, of −1.95 hPa at 26 km, correspond to errors of +8.75% in ozone mixing ratio.

A summary of that analysis is presented in Figure 8 and in Table S4. The pressure offsets reveal themselves most clearly in the middle to upper stratosphere, where they become a significant contribution to the error budget. Below 10 km, the pressure offset errors are typically 1% or less of the ambient pressure. Above 20 km, the offsets appear to be fairly constant with altitude (Figure 8). Radiosonde manufacturers typically cite random and systematic pressure uncertainties of the order of 0.5 hPa, and they recommend applying a pressure correction based on ground-level comparisons between a local barometer and the radiosonde surface pressure measurements. Figure 8 suggests that such a correction may not be helpful by the time the radiosonde reaches the stratosphere; indeed, in the case of the Vaisala RS92, it would be seriously counterproductive. The uncertainty in ozone partial pressure due to pressure uncertainties can be estimated as

$$\varepsilon_{PO} = \frac{\Delta P}{O_3} \nabla_P O_3 \tag{11}$$

where ΔP is the pressure uncertainty. Where ozone partial pressure is converted to mixing ratio using the measured value of P, an additional uncertainty of $\Delta P/P$ should be added. The pressure offset bias is important in the stratospheric portion of the ozone profile and is vanishingly small in the troposphere (Figure 9). Therefore, any correction to account for pressure offsets should be based upon stratospheric measurements.

3.9. Interference From Other Gases

Ozone measurements by the KI method are sensitive to interference by oxidizing or reducing agents (Pitts et al., 1976; Saltzman & Wartburg, 1965; Schenkel & Broder, 1982; Volz & Kley, 1988; Tarasick et al., 2000, 2019b). Although NO_2 and H_2O_2 can cause only modest positive interference, SO_2 can be an important negative interferent. SO_2 causes a quantitative reduction in the ozone detected at 1:1; that is, it cancels ozone mole for mole, and excess SO_2 can accumulate in the cathode solution, affecting ozonesonde measurements well above the polluted boundary layer (De Muer & De Backer, 1993; Komhyr, 1969). While not generally a problem in recent decades, this effect can be an issue near volcanic sources or other large SO_2 emitters such as smelters or power plants (Witte et al., 2018). It can also be used to measure SO_2: Morris et al. (2010) detail an approach that leverages the interference effect in the simultaneous measurement of O_3 and SO_2.

Van Malderen et al. (2016) describe correcting for SO_2 the Brewer-Mast time series but do not estimate the uncertainty of the correction. For modest SO_2 levels, this would be equal to the uncertainty of the SO_2 measurement.

3.10. Total Ozone Normalization

The total ozone normalization factor (N_T) is the ratio of an approximately co-located total ozone column measurement (Ω_C) and the total ozone column derived from the ozonesonde profile (Ω_T):

$$N_T = \frac{\Omega_C}{\Omega_T} \tag{12}$$

where the total ozone column from the ozonesonde (Ω_T) consists of an amount derived by integrating the ozonesonde profile from the surface to balloon burst height (Ω_S) plus an estimated residual ozone column (Ω_R) above the burst altitude; that is

$$\Omega_T = \Omega_S + \Omega_R \tag{13}$$

with

$$\Omega_S = P_0^{-1} \int\limits_{\text{surface}}^{\text{burst}} P_{O3} \, dz \tag{14}$$

The oldest and simplest standard procedure to calculate Ω_R assumes a residual column with constant ozone mixing ratio (CMR) equal to the measured value at the top of the ozonesonde profile. Since the 1970s satellite observations have shown that the ozone mixing ratio is not constant but generally declines above about 35 km. The CMR method therefore tends to overestimate the residual and, depending on the burst altitude, will yield a normalization factor that is about 2–4% too low (McPeters et al., 1997). In addition, uncertainties in the sonde readings of pressure and ozone at the burst altitude can introduce significant uncertainties in the estimation of the residual by this method (e.g., Jeannet et al., 2007). The use of a residual ozone column climatology obtained from satellite observations is now preferred (McPeters & Labow, 2012; McPeters et al., 1997, 2007). However, the influence of uncertainties in pressure readings at the bursting point remains.

The uncertainty of the normalization factor is:

$$\frac{\Delta N_T}{N_T} = \sqrt{\left(\frac{\Delta \Omega_C}{\Omega_C}\right)^2 + \frac{\left(\Delta \Omega_S\right)^2 + \left(\Delta \Omega_R\right)^2}{\left(\Omega_S + \Omega_R\right)^2}} \tag{15}$$

The uncertainties described in 3.1–3.9 vary randomly between soundings, but are assumed to be constant or to vary in a predictable way within a sounding (e.g., with altitude, but not randomly with time). This implies that they are fully correlated in the vertical integral, and the uncertainty of the integral $\Delta \Omega_S$ can therefore be calculated simply as the integral of the uncertainties in the partial pressure from the surface to the balloon burst height

$$\Delta \Omega_S = P_0^{-1} \int\limits_{\text{surface}}^{\text{burst}} \Delta P_{O3} \, dz \tag{16}$$

This neglects any uncertainties that vary randomly during the flights, such as electronic noise or those due to the stochastic nature of bubble formation. As noted in Section 2, these uncertainty components are small and uncorrelated in the vertical integral, and so their contributions to the integral will be relatively small.

From the uncertainties in the satellite residual columns given by McPeters and Labow (2012), the uncertainty $\Delta \Omega_R$ can be similarly calculated (Witte et al., 2018). The uncertainty $\Delta \Omega_C$ can be as low as ± 2–3% but will be higher for scattered-light (e.g., zenith-sky) measurements (Fioletov et al., 2008).

ECC ozonesonde profiles are now not typically normalized, as normalization introduces additional uncertainty ($\Delta \Omega_R$) because the amount of ozone above the balloon burst height can only be estimated. It also renders the ozonesonde record dependent on the total ozone record, an important issue for trend studies, although this concern is alleviated if there is no trend in correction factors. However, the normalization factor provides a useful indicator for the quality of ozonesonde profile data. In routine operation, for ECC ozonesondes that reach at least 30 hPa (24 km), most normalization factors ($\sim$96%) are in the range 0.9%–1.1%, and 99% within 0.8–1.2 (Stauffer, personal communication, 2020).

Table 2
Sources of Ozonesonde Profile Uncertainty Considered in Figures 9 and 10 and Their Estimated Magnitudes

	Uncertainty (1σ)		
Source	Midlatitude (Edmonton)	Tropical (Watukosek)	Confidence
Stoichiometry η_C	±3.0%	±3.0%	Low
T_P measurement	±0.3%	±0.5%	High
Φ_{PM} measurement	±1.0%	±1.0%	High
Φ_{PM} RH correction	±0.5%	±0.5%	Moderate
Current measurement (interface)	±1.0%	±1.0%	High
η_P pump efficiency correction	JMA; see Figure 3	JMA; see Figure 3	High
η_A absorption efficiency	±1% ± 1%*P/P_0 (2.5 ml solution)	±1%	Moderate
Background current	0.02 μA	0.02 μA	Low
Ascent rate variation	±12%*$e^{-\Delta t/\tau}\nabla_t O_3$	±12%*$e^{-\Delta t/\tau}\nabla_t O_3$	High
Pressure offset	±1.0 hPa	±1.0 hPa	Moderate
Total ozone normalization factor	5.2% (7.9%)	5.2% (5.2%)	High

Note. Total ozone normalization factor uncertainties are calculated for a balloon bursting at 30 km in June, and at 25 km in January (in parentheses). See text for details.

Note that the biases previously discussed can also have a large effect on the calculated normalization factor (e.g., pressure offsets). Where biases are largely independent of altitude, normalization may improve sonde accuracy by approximately removing a mean bias, but in this case the uncertainty of the normalization factor must be added to the estimated uncertainty at each point of the profile; that is, the uncertainty of each point becomes

$$\frac{\Delta P_{O3}^N}{P_{O3}^N} = \sqrt{\left(\frac{\Delta P_{O3}}{P_{O3}} - \frac{\Delta \Omega_S}{\Omega_S}\right)^2 + \left(\frac{\Delta N_T}{N_T}\right)^2} \qquad (17)$$

which for random errors will always be larger than the uncertainty of the uncorrected profile. The quantities on the right-hand side refer to the nonnormalized data.
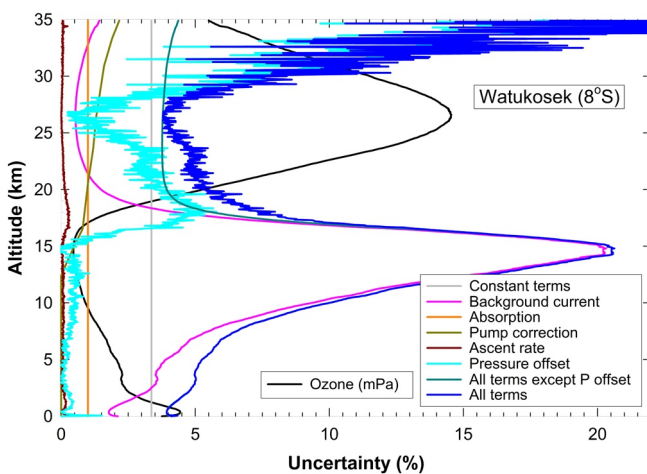

Figure 10. Uncertainty analysis for a tropical station (Watukosek, Java), showing the influence of different uncertainty terms, for the assumed values in Table 2. Because of the very low ozone in the tropical upper troposphere, the uncertainty due to the background current dominates at these altitudes.

3.11. Two Examples of Uncertainty Budgets

Average uncertainties as a function of altitude are calculated for a typical midlatitude site (Edmonton, Canada, 53°N), and a tropical site (Watukosek, Java, 8°S), following the estimates for each source discussed above. Details are given in Table 2. All quoted uncertainties are one standard deviation (1σ). It is clear that while the background current uncertainty is important in the upper troposphere at midlatitudes (Figure 9), it dominates in the upper tropical troposphere (Figure 10), even though the assumed value of 0.02 μA is small (Table 1). In both cases the uncertainty due to pressure bias, for sondes without GPS altitude registration, dominates at altitudes above 25 km. Several smaller terms that are not altitude-dependent are combined in the gray line "Constant terms"; this includes uncertainties in pump temperature and initial flow rate calibration, as well as the current measurement, but is dominated by the assumed uncertainty of the stoichiometry (3%). As noted in Section 3.3, this may be an overestimate between 12 and 25 km, where the empirical curves from intercomparisons show smaller variances; however, it is likely to be an underestimate at higher altitudes where the stoichiometry is more affected by the slow response (Equation 5). Note that the sondes in

the JOSIE and Vanscoy intercomparisons were compared to a common pressure sensor, so these curves do not include any variance due to pressure offsets.

4. Outstanding Issues: Recommendations for Future Research

From the foregoing analysis it is clear that there are several significant sources of uncertainty that may be reduced with further research, as well as several others that may be eliminated by adherence to recommended standard operating procedures. Consistent SOP use will eliminate some of the largest sources of uncertainty (the ENSCI 1% KI correction uncertainty) as well as some smaller contributions (e.g. the 2.5 ml solution correction uncertainty). The largest remaining sources of uncertainty in Table 1 are also the most poorly understood; viz. conversion efficiency and background current, and so should be considered high priority for further research, as the most significant impediments to achieving the goal of 5% overall accuracy.

4.1. Conversion Efficiency and Stoichiometry of the O_3 +KI Reaction

Modern benchtop ozone calibrators render many experiments simple that were difficult in the past. More experiments are needed to better understand, or at least predict, the behavior of the ECC sensor with respect to time and ozone exposure. Both its temporal response (time constants) and the impact of the phosphate buffer and solution strength should be characterized, for each sensor model. Better uncertainty estimates for the stoichiometry of Reaction R1 can be derived, as well as variability of the time constants of the slow (20 min time constant) and fast reaction pathways.

It is not known whether sensor response time is constant, or varies with sensor model, or from ozonesonde to ozonesonde. If the latter, then the sensor decay test information (from sonde preparation checkout sheets) may provide useful information for reanalysis of older records.

The effects of interfering gases with the KI reaction are known primarily from laboratory work, in glass vessels, that predates modern ECC sondes. There is some evidence that the degree of interference may be different in an ECC sonde (Tarasick et al., 2000). Interference by ammonia is occasionally suggested (Anfossi et al., 1991), but not quantified. Although heterogeneous ozone loss on mineral dust is well known (Bonasoni et al., 2004; Chang et al., 2005; Mogili et al., 2006), interference with electrochemical sondes has been thought to be negligible (Andry et al., 2014; Rosen, 1968). It is not evident in simultaneous launches of aerosol sondes (H. Vömel, private communication), but dust effects on ECC sondes have not been explored systematically.

4.2. New Pump Efficiencies

While it is clear that the older pump efficiency tables (Komhyr, 1986; Komhyr et al., 1995) should be retired and replaced by the more recent experimentally obtained tables (Johnson et al., 2002; Nakano, personal communication, 2019), this will result in an overestimate of ozone, owing to the increase of stoichiometry that is compensated by the Komhyr pump corrections (Figure 4). A prerequisite to using accurate pump corrections is that the conversion efficiency as a function of pressure first be measured under a variety of conditions, in the WCCOS environmental chamber. As a large data set of appropriate measurements exists from past JOSIE campaigns, it may be possible to derive suitable profiles of η_C from existing data. The extent to which these profiles vary for different sounding conditions remains to be determined. It is also not clear whether the effort of measuring individual pump flow efficiencies at each site, for each sonde, would yield significant improvements in uncertainty (over the use of an average table). The accuracy (repeatability) of the pump measurement needs to be determined.

4.3. Background Current

While we have suggested that to a large degree, the background current is a manifestation of the slow secondary response of the ECC sensor, this has not been unequivocally established. The work suggested in Sections 4.1 and 4.2 will also help determine whether even after correction for the slow secondary response,

a constant (or decaying) initial offset is needed to account for issues like NO_2 interference or a leaky ion bridge.

4.4. Radiosonde Pressure Measurements

While this is the dominant error source above the lower stratosphere (Figure 9), it can be largely eliminated by the use of GPS-equipped radiosondes. This should be part of SOPs in the future. It is not clear how to correct older data for radiosonde pressure errors, in the absence of a more accurate GPS measurement of altitude, although larger offsets may reveal themselves by nonlinearity in the apparent balloon rise rate or unrealistic mixing ratios at higher altitudes (Stauffer et al., 2014). Sterling et al. 2018 have also suggested comparing temperature profiles from nearby meteorological soundings to the temperature profile measured by the ozonesonde package as a way to detect pressure offsets. In the absence of a robust method to correct for pressure biases, they should be treated as a random uncertainty as described in Equation 11.

Fortunately, most or all newer radiosondes use GPS sensors with typical accuracies in height in the stratosphere of ±20 m (da Silveira et al., 2006; Nash et al., 2006, 2011), which will reduce this source of error in future to the insignificant range of 0.1%–0.3% in ozone.

Care must be taken with the differences between geometric height (the native coordinate for GPS) and geopotential height, as well as with the formula used for the conversion of pressure or geometric height to geopotential height (i.e., a constant or latitude-dependent acceleration of gravity, *g*). In either case the difference can be about 150 m at 30 km altitude, or ~2% in ozone. Even such modest changes, if systematic, can affect trend calculations.

4.5. Total Ozone Normalization Factor

This is largely dependent on the stratospheric column, as this contains the major fraction of the total ozone amount, and the tropospheric portion of the profile may be poorly represented (Morris et al., 2013). The use of sonde data above 10 hPa may also introduce larger errors. Although normalization of ECC sonde profiles is no longer recommended (Smit & ASOPOS Panel, 2014), these questions have never been systematically addressed. This could be done using existing JOSIE UV-photometer data. Such a study is recommended, as it may provide useful insight into the value of N_T as a data quality indicator.

4.6. Instrument Biases

ECC-ozonesondes have gone through several modifications of the instrument and procedures since they were first manufactured in the early 1970s (Johnson et al., 2002). These changes, if they introduce new systematic uncertainties in any of the parameters in Equation 1, may cause significant uncertainties in ozonesonde trend analysis (SPARC-IOC-GAW, 1998).

The differences found between the ENSCI-Z ozonesonde and the SPC-6A ozonesonde (Deshler et al., 2017; Smit et al., 2007) demonstrate that the conversion efficiency (η_C) can be different for apparently modest differences in sonde construction, and so may be different for other changes in manufacture or in preparation. Such changes will need to be carefully tracked by the sonde community so that ozonesonde data are reliable, that is, free from artifacts or drift, as a transfer standard for comparing and merging satellite time series, and for long-term trend analyses. Intercomparison data indicate that other changes to ECC response have been modest, in the troposphere (Tarasick et al., 2019b), and the lack of significant trends in total ozone normalization factors at most sites suggests that they have been small in the stratosphere as well.

Ozonesonde-satellite comparisons may also detect biases among ozonesonde profiles measured at various stations, presumably due to differences in ozonesonde instrument type and preparation (Thompson et al., 2017; Witte et al., 2017). This was noted when total ozone measured by tropical ozonesondes at various SHADOZ sites was compared to total ozone from the nadir viewing BUV satellite instruments, TOMS and OMI (Thompson et al., 2007, 2012). Recent changes relative to satellite data have been observed at a number of stations in the global network (Stauffer et al., 2020). The comprehensive analysis of Hubert et al. (2016),

comparing sonde results to 14 satellite sensors, is a particularly valuable approach, and should be performed regularly. Comparisons with IAGOS aircraft data (Staufer et al., 2013, 2014; Tanimoto et al., 2015; Tarasick et al., 2019b; Zbinden et al., 2013) can independently detect tropospheric biases.

It is imperative that sonde intercomparisons (Attmannspacher & Dütsch, 1970, 1981; Deshler et al., 2008; Hilsenrath et al., 1986; Kerr et al., 1994; Smit et al., 2007) continue to be held regularly, and that these be related to the modern UV-absorption standard (BIPM, 2019; Tarasick et al., 2019b).

4.7. Re-Used Ozonesondes

Current experience with re-using ozonesondes shows that recuperated ozonesondes can be re-used and perform well, after careful cleaning and testing in the laboratory (Van Malderen et al., 2014). However, currently there are no quality assurance standards for refurbished sensors, and a number of ozonesonde sites fly refurbished ozonesondes using manufacturer SOPs or their own set of SOPs. It is recommended that universal SOPs be developed and promulgated. In addition, the uncertainties of re-used ozonesondes versus new ozonesondes should be evaluated, especially with respect to background currents, pump corrections, and conversion efficiency.

4.8. Ozone Destruction Filters

While background current is measured at the launch site ideally by sampling laboratory-grade ozone-free ("zero") air, this is not always available at remote sounding sites, and so must be produced by passing ambient air passing through an ozone filter. These are generally commercial filters containing hopcalite (a mixture of copper and manganese oxides, which catalyzes the conversion of ozone to ordinary oxygen), or charcoal. The efficiency of these filters at removing ozone is assumed to be 100%, but this may not be true in all environments. Although most operators replace them periodically, it is not well known how they may degrade with time. They are thought to degrade somewhat rapidly in very humid tropical environments. It is not known to what extent they remove NO_2. It is recommended that a comprehensive study be undertaken to better quantify this potential source of error.

It is further recommended that the ASOPOS panel develop detailed specifications for the quality and reliability of ozonesonde preparation equipment: for example, bench testers, and the other instruments used to record RH_{Lab}, P_{Lab}, and T_{Lab}.

5. Conclusions

The accuracy and stability of the ECC sonde record has made it very valuable for long-term trend analysis, and as a transfer standard for satellite validation and for comparing and merging different satellite records. This importance implies that more effort should be placed on understanding and reducing ECC sonde uncertainties. While spatial inhomogeneity has been reduced, and the overall accuracy of the global ozonesonde network improved, by adopting strict standard operating procedures (Smit & ASOPOS Panel, 2014), there is more that can be achieved by improving SOPs and homogenizing the historical record. Efforts to date (e.g., Sterling et al., 2018; Tarasick et al., 2016; Thompson et al., 2017; 2019; van Malderen et al., 2016; Witte et al., 2017; 2019) have reduced both stratospheric and tropospheric biases, and improved agreement with coincident total ozone measurements. New merged global data sets (Hassler et al., 2018; McPeters & Labow, 2012; Moeini et al., 2019) that include ozonesonde data additionally justify this effort.

These continuing efforts should proceed in tandem with research, described herein, to better quantify and understand systematic and random uncertainty in ECC data, and to closely monitor systematic changes in response. We have presented a "roadmap" of issues, recommendations, and solutions to bring ECC accuracy to the 5% level. This appears to be quite achievable, with international effort.

The major remaining sources of uncertainty, in large part because they are poorly understood, are stoichiometry and background current. Fortunately, these can be well addressed by suitable experiments using the

WCCOS facility. They should be considered high priority for further research. At the same time there are questions related to the effects of total ozone normalization, or equivalently, its characterization as a data quality indicator, that could be answered with the same data.

We have made specific recommendations, which we summarize here:

1) Stations should follow strictly the ASOPOS recommendations (Smit & ASOPOS Panel, 2014; Smit et al., 2020); however, changes to SOPs, including those that may be recommended by future ASOPOS panels, must be carefully documented so that their effects on ozone time series can be estimated and corrected.
2) Conversion efficiency (η_C) should be measured as a function of pressure and temperature, in the WCCOS chamber, for different models of sondes from both manufacturers. While it is hoped that this may lead to better understanding of the stoichiometry in the cell, the primary objective is to empirically characterize η_C and its uncertainty and variation with altitude, under a range of conditions. This may also eliminate the need for empirical bias corrections (e.g., Deshler et al., 2017).
3) The sonde response model of Section 3.4 should be investigated in the same manner with existing data from past WCCOS chamber (JOSIE) experiments.
4) Pump flow efficiencies should be characterized in a more systematic fashion, with regard to uncertainties, repeatability, and variability with model, manufacturer, and batch of sondes.
5) The relationship of the total ozone normalization factor to the ozonesonde profile, and therefore its value as a data quality indicator, should be systematically investigated. This could be done using existing JOSIE data.
6) Universal SOPs for re-used ozonesondes should be developed and published. In addition, the uncertainties of re-used ozonesondes versus new ozonesondes should be evaluated (Smit et al., 2020).
7) The behavior of commonly used ozone destruction filters should be investigated, with regard to efficiency, sensitivity to contaminants, and degradation with time.
8) The detection of artifacts in ozonesonde time series should be a priority for the global network (Stauffer et al., 2020). More ancillary data, such as pump motor voltage, current, speed, and cell temperature should be routinely recorded. Stronger communication with ECC manufacturers would be of mutual benefit, if it can be achieved despite proprietary limitations.

Finally, the importance of regular sonde intercomparisons, employing UV standard instruments traceable to the modern UV-absorption standard, such as through the WCCOS facility, cannot be overemphasized. It is essential to detect and quantify any systematic changes in response (biases) that could affect the integrity of ozonesonde records, and the reliability of ozonesonde time series for merging shorter satellite data sets and for evaluation of satellite sensor drift. Regular comparison with multiple satellite sensors will be a valuable tool for detection of such artifacts, while the WCCOS facility can help understand them.

Data Availability Statement

No new measurements were made for this review article. All data sets discussed in the text were obtained from the published scientific literature. Ozonesonde data used in this publication are publicly available, from the World Ozone and UV Data Centre (http://www.woudc.org).

References

Andrey, J., Cuevas, E., Parrondo, M. C., Alonso-Pérez, S., Redondas, A., & Gil-Ojeda, M. (2014). Quantification of ozone reductions within the Saharan air layer through a 13-year climatologic analysis of ozone profiles. *Atmospheric Environment*, *84*, 28–34. https://doi.org/10.1016/j.atmosenv.2013.11.030

Anfossi, D., Sandroni, S., & Viarengo, S. (1991). Tropospheric ozone in the nineteenth century: The Moncalieri series. *Journal of Geophysical Research*, *96*, 17349–17352.

Antón, M., López, M., Vilaplana, J. M., Kroon, M., McPeters, R., Bañón, M., & Serrano, A. (2009). Validation of OMI-TOMS and OMI-DOAS total ozone column using five Brewer spectroradiometers at the Iberian peninsula. *Journal of Geophysical Research*, *114*, D14307. https://doi.org/10.1029/2009JD012003

Attmannspacher, A., & Dütsch, H. U. (1970). International ozone sonde intercomparison at the Observatory Hohenpeissenberg. *Berichte des Deutschen Wetterdienstes*, *120*, 1–85.

Attmannspacher, A., & Dütsch, H. U. (1981). Second international ozone sonde intercomparison at the Observatory Hohenpeissenberg. *Berichte des Deutschen Wetterdienstes*, *157*, 1–64.

Bergshoeff, G., Lanting, R. W., Prop, J. M. G., & Reynders, H. F. R. (1980). Improved neutral buffered potassium iodide method for ozone. *Analytical Chemistry*, *52*, 541–546.

BIPM. (2019). Retrieved from http://www.bipm.org/en/bipm/chemistry/gas-metrology/ozone.html

Bojkov, R. D., & Fioletov, V. E. (1997). Changes of the lower stratospheric ozone over Europe and Canada. *Journal of Geophysical Research*, *102*, 1337–1347. https://doi.org/10.1029/96JD00095

Bonasoni, P., Cristofanelli, P., Calzolari, F., Bonafè, U., Evangelisti, F., Stohl, A., et al. (2004). Aerosol-ozone correlations during dust transport episodes. *Atmospheric Chemistry and Physics*, *4*, 1201–1215. https://doi.org/10.5194/acp-4-1201-2004

Bowen, I. G., & Regener, V. H. (1951). On the automatic chemical determination of atmospheric ozone. *Journal of Geophysical Research*, *56*(3), 307–324. https://doi.org/10.1029/JZ056i003p00307

Boyd, A. W., Willis, C., & Cyr, R. (1970). New determination of stoichiometry of the iodometric method for ozone analysis at pH 7.0. *Analytical Chemistry*, *42*(6), 670–672. https://doi.org/10.1021/ac60288a030

Boyd, I., Bodeker, G., Connor, B., Swart, D., & Brinksma, E. (1998). An assessment of ECC ozone sondes operated using 1% and 0.5% KI cathode solutions at Lauder, New Zealand. *Geophysical Research Letters*, *25*, 2409–2412.

Boynard, A., Clerbaux, C., Coheur, P.-F., Hurtmans, D., Turquety, S., George, M., et al. (2009). Measurements of total and tropospheric ozone from IASI: Comparison with correlative satellite, ground-based and ozonesonde observations. *Atmospheric Chemistry and Physics*, *9*, 6255–6271. https://doi.org/10.5194/acp-9-6255-2009

Brewer, A. W., & Milford, J. R. (1960). The Oxford-Kew ozone sonde. *Proceedings of the Royal Society of London, Series A, 256*, 470–495.

Byers, D. H., & Saltzman, B. E. (1959). Determination of ozone in air by neutral and alkaline iodide procedures. *Advances in Chemistry*, *21*, 93–101.

Chang, R. Y.-W., Sullivan, R. C., & Abbatt, J. P. D. (2005). Initial uptake of ozone on Saharan dust at atmospheric relative humidities. *Geophysical Research Letters*, *32*, L14815. https://doi.org/10.1029/2005GL023317

Cooper, O. R., Parrish, D. D., Stohl, A., Trainer, M., Nédélec, P., Thouret, V., et al. (2010). Increasing springtime ozone mixing ratios in the free troposphere over western North America. *Nature*, *463*, 344–348. https://doi.org/10.1038/nature08708

Cooper, O. R, Stohl, A., Trainer, M., Thompson, A., Witte, J. C., Oltmans, S. J., et al. (2006). Large upper tropospheric ozone enhancements above mid-latitude North America during summer: In situ evidence from the IONS and MOZAIC ozone measurement network. *Journal of Geophysical Research*, *111*, D24S05. https://doi.org/10.1029/2006JD007306

Dabberdt, W. F., Shellhorn, R., Cole, H., Paukkunen, A., Horhammer, J., & Antikainen, V. (2005). *Radiosondes*. In J.Holton, J.Pyle, & J.Curry (Eds.), Encyclopedia of atmospheric sciences (5, pp. 1900–1913). London: Academic Press.

da Silveira, R. B., Fisch, G. F., Machado, L. A. T., Dall'Antonia, A. M., Sapucci, L. F., Fernandes, D., et al. (2006). *WMO intercomparison of GPS radiosondes*. Alcantara, Brazil, 20 May–10 June 2001 WMO/TD–No. 1314, p. 65. Retrieved from http://www.wmo.int/pages/prog/www/IMOP/publications/IOM-90_RSO-Brazil/IOM-90_RSO_EMA_Alcantara2001.pdf

Davies, J., McElroy, C. T., Tarasick, D. W., & Wardle, D. I. (2003). *Ozone capture efficiency in ECC Ozonesondes; measurements made in the laboratory and during Balloon Flights*. EGS-AGU-EUG Joint Assembly, Abstracts from the meeting held in Nice, France, 6–11 April 2003. Abstract id: 13703.

De Muer, D., & De Backer, H. (1993). Influence of sulfur dioxide trends on Dobson measurements and on electrochemical ozone soundings. In T.Hendriksen (Ed.), *Atmospheric ozone, Proc. SPIE 2047* (pp. 18–26).

De Muer, D., & Malcorps, H. (1984). The frequency response of an electrochemical ozone sonde and its application to the deconvolution of ozone profiles. *Journal of Geophysical Research*, *89*, 1361–1372.

Deshler, T., Mercer, J., Smit, H. G. J., Stuebi, R., Levrat, G., Johnson, B. J., et al. (2008). Atmospheric comparison of electrochemical cell ozonesondes from different manufacturers, and with different cathode solution strengths: The Balloon Experiment on Standards for Ozonesondes. *Journal of Geophysical Research*, *113*, D04307. https://doi.org/10.1029/2007JD008975

Deshler, T., Stübi, R., Schmidlin, F. J., Mercer, J. L., Smit, H. G. J., Johnson, B. J., et al. (2017). Methods to homogenize ECC ozonesonde measurements across changes in sensing solution concentration or ozonesonde manufacturer. *Atmospheric Measurement Techniques*, *10*, 2012–2043. https://doi.org/10.5194/amt-10-2021-2017

Dietz, R. N., Pruzansky, J., & Smith, J. D. (1973). Effect of pH on the stoichiometry of the iodometric determination of ozone. *Analytical Chemistry*, *45*, 402–404.

Ehmert, A. (1951). Ein einfaches Verfahren zur absoluten Messung des Ozongehalts der Luft. *Meteorologische Rundschau*, *4*, 64–68.

Fioletov, V. E., Kerr, J. B., Wardle, D. I., Davies, J., Hare, E. W., McElroy, C. T., & Tarasick, D. W. (1997). Long-term decline of ozone over the Canadian Arctic to early 1997 from ground-based and balloon sonde measurements. *Geophysical Research Letters*, *24*, 2705–2708.

Fioletov, V. E., Labow, G., Evans, R., Hare, E. W., Köhler, U., McElroy, C. T., et al. (2008). Performance of the ground-based total ozone network assessed using satellite data. *Journal of Geophysical Research*, *113*, D14313. https://doi.org/10.1029/2008JD009809

Fioletov, V. E., Tarasick, D. W., & Petropavlovskikh, I. (2006). Estimating ozone variability and instrument uncertainties from SBUV(/2), ozonesonde, Umkehr, and SAGE II measurements: Short-term variations. *Journal of Geophysical Research*, *111*, d02305. https://doi.org/10.1029/2005JD006340

Flamm, D. L. (1977). Analysis of ozone at low concentrations with boric acid buffered KI. *Environmental Science and Technology*, *11*, 879–983.

Fortuin, J., & Kelder, H. (1998). An ozone climatology based on ozonesonde and satellite measurements. *Journal of Geophysical Research*, *103*, 31709–31733.

Glückauf, E. (1944) The ozone content of surface air and its relation to some meteorological conditions. *Quarterly Journal Royal Meteorological Society*, *70*, 13–21. https://doi.org/10.1002/qj.49707030303

GRUAN. (2019). *Gruan Ozonesonde Technical Document*. Retrieved from https://acd-ext.gsfc.nasa.gov/anonftp/acd/shadoz/nletter/GruanOzonesondeGuide_1.1.0.3_GEB_JCW.pdf

Harder, J. (1987). *Measurement of springtime Antarctic ozone depletion and development of a balloon borne ultraviolet photometer* (Ph.D. thesis). Laramie: Dept. of Phys. and Astron., Univ. of Wyoming.

Harris, N. R. P., Hassler, B., Tummon, F., Bodeker, G., Hubert, D., Petropavlovskikh, I., et al. (2015). Past changes in the vertical distribution of ozone – Part 3: Analysis and interpretation of trends. *Atmospheric Chemistry and Physics*, *15*, 9965–9982. https://doi.org/10.5194/acp-15-9965-2015

Hassler, B., Kremser, S., Bodeker, G. E., Lewis, J., Nesbit, K., Davis, S. M., et al. (2018). An updated version of a gap-free monthly mean zonal mean ozone database. *Earth System Science Data*, *10*, 1473–1490. https://doi.org/10.5194/essd-10-1473-2018

Hassler, B., Petropavlovskikh, I., Staehelin, J., August, T., Bhartia, P. K., Clerbaux, C., et al. (2014). Past changes in the vertical distribution of ozone – Part 1: Measurement techniques, uncertainties and availability. *Atmospheric Measurement Techniques*, *7*, 1395–1427. https://doi.org/10.5194/amt-7-1395-2014

Hilsenrath, E., Attmannspacher, W., Bass, A., Evans, W., Hagemeyer, R., Barnes, R. A., et al. (1986). Results from the balloon intercomparison campaign (BOIC). *Journal of Geophysical Research*, *91*, 13137–13152.

Hocking, W. K., Carey-Smith, T. K., Tarasick, D. W., Argall, P. S., Strong, K., Rochon, Y., et al. (2007). Detection of stratospheric ozone intrusions by windprofiler radars. *Nature*, *450*(7167), 281–284. https://doi.org/10.1038/nature06312

Hodges, J. T., Viallon, J., Brewer, P. J., Drouin, B. J., Gorshelev, V., Janssen, C., et al. (2019). Recommendation of a consensus value of the ozone absorption cross-section at 253.65 nm based on a literature review. *Metrologia*, *56*, 034001. https://iopscience.iop.org/article/10.1088/1681-7575/ab0bdd

Hodgeson, J. A., Baumgardner, R. E., Martin, B. E., & Rehme, K. A. (1971). Stoichiometry in the neutral iodometric procedure for ozone by gas phase titration with nitric oxide. *Analytical Chemistry*, *43*(8), 1123–1126. https://doi.org/10.1021/ac60303a026

Hoogen, R., Rozanov, V. V., & Burrows, J. P. (1999). Ozone profiles from GOME satellite data: Algorithm description and first validation. *Journal of Geophysical Research*, *104*(D7), 8263–8280. https://doi.org/10.1029/1998JD100093

Huang, L. J., Chen, M. J., Lai, C. H., Hsu, H. T., & Lin, C. H. (2015). New Data Processing Equation to Improve the Response Time of an Electrochemical Concentration Cell (ECC) Ozonesonde. *Aerosol and Air Quality Research*, *15*, 935–944. https://doi.org/10.4209/aaqr.2014.05.0097

Hubert, D., Lambert, J.-C., Verhoelst, T., Granville, J., Keppens, A., Baray, J.-L., et al. (2016). Ground-based assessment of the bias and long-term stability of 14 limb and occultation ozone profile data records. *Atmospheric Measurement Techniques*, *9*, 2497–2534. https://doi.org/10.5194/amt-9-2497-2016

Inai, Y., Shiotani, M., Fujiwara, M., Hasebe, F., & Vömel, H. (2015). Altitude misestimation caused by the Vaisala RS80 pressure bias and its impact on meteorological profiles. *Atmospheric Measurement Techniques*, *8*(10), 4043–4054. https://doi.org/10.5194/amt-8-4043-2015

Jeannet, P., Stübi, R., Levrat, G., Viatte, P., & Staehelin, J. (2007). Ozone balloon soundings at Payerne (Switzerland): Reevaluation of the time series 1967–2002 and trend analysis, *J. Geophys. Res.*, *112*(D11302), https://doi.org/10.1029/2005JD006862

Johnson, B. J., Oltmans, S. J., Vömel, H., Smit, H. G. J., Deshler, T., & Kroeger, C. (2002). ECC ozonesonde pump efficiency measurements and tests on the sensitivity to ozone of buffered and unbuffered ECC sensor cathode solutions. *Journal of Geophysical Research*, *107*, D19. https://doi.org/10.1029/2001JD000557

Kerr, J. B., Fast, H., McElroy, C. T., Oltmans, S. J., Lathrop, J. A., Kyro, E., et al. (1994). The 1991 WMO international ozonesonde intercomparison at Vanscoy, Canada. *Atmosphere-Ocean*, *32*, 685–716.

Kivi, R., Kyrö, E., Turunen, T., Harris, N. R. P., von der Gathen, P., Rex, M., et al. (2007). Ozonesonde observations in the Arctic during 1989 – 2003: Ozone variability and trends in the lower stratosphere and free troposphere. *Journal of Geophysical Research*, *112*, D08306. https://doi.org/10.1029/2006JD007271

Kley, D., Crutzen, P. J., Smit, H. G. J., Vömel, H., Oltmans, S. J., Grassl, H., & Ramanathan, V. (1996). Observations of near-zero ozone levels over the convective Pacific: Effects on air chemistry. *Science*, *274*, 230–233.

Komhyr, W. D. (1967). Nonreactive gas sampling pump. *Review of Scientific Instruments*, *38*, 981–983.

Komhyr, W. D. (1969). Electrochemical concentration cells for gas analysis. *Annales Geophysicae*, *25*, 203–210.

Komhyr, W. D. (1986). *Operations handbook-Ozone measurements to 40-km altitude with model 4A electrochemical concentration cell (ECC) ozonesondes (used with 1680 MHz radiosondes)*. NOAA Tech. Memo. ERL ARL-149, Boulder, CO: Air Resour. Lab.

Komhyr, W. D., Barnes, R. A., Brothers, G. B., Lathrop, J. A., & Opperman, D. P. (1995). Electrochemical concentration cell ozonesonde performance evaluation during STOIC 1989. *Journal of Geophysical Research*, *100*(D5), 9231–9244. https://doi.org/10.1029/94JD02175

Komhyr, W. D., & Harris, T. B. (1971). *Development of an ECC-Ozonesonde*. NOAA Techn. Rep. ERL 200-APCL 18. Boulder, CO: U.S. G.P.O.

Kopczynski, S. L., & Bufalini, J. J. (1971). Some observations on stoichiometry of iodometric analyses of ozone at pH 7.0. *Analytical Chemistry*, *43*, 1126–1127.

Lamsal, L., Weber, M., Tellmann, S., & Burrows, J. (2004). Ozone column classified climatology of ozone and temperature profiles based on ozonesonde and satellite data. *Journal of Geophysical Research*, *109*, D20304. https://doi.org/10.1029/2004JD004680

Lanting, R. W. (1979). Modification of the potassium iodide procedure for improved stoichiometry. *Atmospheric Environment*, *13*, 553–554.

Lin, M., Horowitz, L. W., Oltmans, S. J., Fiore, A. M., & Fan, S. (2014). Tropospheric ozone trends at Mauna Loa Observatory tied to decadal climate variability. *Nature Geoscience*, *7*, 136–143. https://doi.org/10.1038/ngeo2066

Liu, G., Liu, J. J., Tarasick, D. W., Fioletov, V. E., Jin, J. J., Moeini, O., et al. (2013). A global tropospheric ozone climatology from trajectory-mapped ozone soundings. *Atmospheric Chemistry and Physics*, *13*, 10659–10675. https://doi.org/10.5194/acp-13-10659-2013

Liu, G., Tarasick, D. W., Fioletov, V. E., Sioris, C. E., & Rochon, Y. J. (2009). Ozone correlation lengths and measurement uncertainties from analysis of historical ozonesonde data in North America and Europe. *Journal of Geophysical Research*, *114*, D04112. https://doi.org/10.1029/2008JD010576

Liu, J., Tarasick, D. W., Fioletov, V. E., McLinden, C., Zhao, T., Gong, S., et al. (2013). A global ozone climatology from ozone soundings via trajectory mapping: A stratospheric perspective. *Atmospheric Chemistry and Physics*, *13*, 11441–11464. https://doi.org/10.5194/acp-13-11441-2013

Liu, X., Chance, K., Sioris, C. E., Spurr, R. J. D., Kurosu, T. P., Martin, R. V., & Newchurch, M. J. (2005). Ozone profile and tropospheric ozone retrievals from the Global Ozone Monitoring Experiment: Algorithm description and validation. *Journal of Geophysical Research*, *110*, D20307. https://doi.org/10.1029/2005JD006240

Logan, J. (1994). Trends in the vertical distribution of ozone: An analysis of ozonesonde data. *Journal of Geophysical Research*, *99*, 25553–25585.

Logan, J. A. (1999). An analysis of ozonesonde data for the troposphere: Recommendations for testing 3-D models and development of a gridded climatology for tropospheric ozone. *Journal of Geophysical Research*, *104*, 16115–16149.

Logan, J. A., Megretskaia, I. A., Miller, A. J., Tiao, G. C., Choi, D., Zhang, L., et al. (1999). Trends in the vertical distribution of ozone: A comparison of two analyses of ozonesonde data. *Journal of Geophysical Research*, *104*, 26373–26400.

Logan, J. A., Staehelin, J., Megretskaia, I. A., Cammas, J. P., Thouret, V., Claude, H., et al. (2012). Changes in ozone over Europe: Analysis of ozone measurements from sondes, regular aircraft (MOZAIC) and alpine surface sites. *Journal of Geophysical Research*, *117*, D09301. https://doi.org/10.1029/2011JD016952

Manney, G. L., Santee, M. L., Rex, M., Livesey, N. J., Pitts, M. C., Veefkind, P., et al. (2011). Unprecedented Arctic ozone loss in 2011. *Nature*, *478*, 469–475. https://doi.org/10.1038/nature10556

McPeters, R. D., Frith, S., & Labow, G. J. (2015). OMI total column ozone: Extending the long-term data record. *Atmospheric Measurement Techniques*, *8*, 4845–4850. https://doi.org/10.5194/amt-8-4845-2015

McPeters, R., Kroon, M., Labow, G., Brinksma, E., Balis, D., Petropavlovskikh, I., et al. (2008). Validation of the Aura ozone monitoring instrument total column ozone product. *Journal of Geophysical Research*, *113*, D15S14. https://doi.org/10.1029/2007JD008802

McPeters, R. D., & Labow, G. J. (2012). Climatology 2011: An MLS and sonde derived ozone climatology for satellite retrieval algorithms. *Journal of Geophysical Research*, *117*(D10), D10303. https://doi.org/10.1029/2011jd017006

McPeters, R. D., Labow, G. J., & Johnson, B. J. (1997). A satellite-derived ozone climatology for balloonsonde estimation of total column ozone. *Journal of Geophysical Research*, *102*, 8875–8886. https://doi.org/10.1029/96JD02977

McPeters, R. D., Labow, G. J., & Logan, J. A. (2007). Ozone climatological profiles for satellite retrieval algorithms. *Journal of Geophysical Research*, *112*, D05308. https://doi.org/10.1029/2005JD006823

Miles, G. M., Siddans, R., Kerridge, B. J., Latter, B. G., & Richards, N. A. D. (2015). Tropospheric ozone and ozone profiles retrieved from GOME-2 and their validation. *Atmospheric Technology*, *8*, 385–398. https://doi.org/10.5194/amt-8-385-2015

Moeini, O., Puetz, C., Degenstein, D. A., Tarasick, D. W., Bourassa, A. E., Plummer, D. A., & Rochon, Y. J. (2019). *Ozone trends in the stratosphere using the merged Ozonesonde/SAGE II/OSIRIS/OMPS ozone profiles dataset, A54H-03, presented at 2019 Fall Meeting*. San Francisco, CA: AGU.

Moeini, O., Tarasick, D. W., McElroy, C. T., Liu, J., Osman, M. K., Thompson, A. M., et al. (2020). Estimating boreal fire-generated ozone over North America using ozonesonde profiles and a differential back trajectory technique. *Atmospheric Environment: X*, *7*, 100078. https://doi.org/10.1016/j.aeaoa.2020.100078

Mogili, P. K., Kleiber, P. D., Young, M. A., & Grassian, V. H. (2006). Heterogeneous uptake of ozone on reactive components of mineral dust aerosol: An environmental aerosol reaction chamber study. *The Journal of Physical Chemistry A*, *110*(51), 13799–13807. https://doi.org/10.1021/jp063620g

Morris, G., Komhyr, W. D., Hirokawa, J., Flynn, J., Lefer, B., Krotokov, N., & Ngan, F. (2010). A balloon sounding technique for measuring SO_2 plumes, *Journal of Atmospheric and Oceanic Technology*, *27*, 1318–1330. https://doi.org/10.1175/2010JTECHA1436.1

Morris, G. A., Labow, G., Akimoto, H., Takigawa, M., Fujiwara, M., Hasebe, F., et al. (2013). On the use of the correction factor with Japanese ozonesonde data. *Atmospheric Chemistry and Physics*, *13*(3), 1243–1260. https://doi.org/10.5194/acp-13-1243-2013

Murray, F. W. (1967). On the computation of saturation vapour pressure. *Journal of Applied Meteorology*, *6*, 203–204.

Nash, J., Oakley, T., Vömel, H., & Wei, L. (2011). *WMO inter-comparison of high quality radiosonde systems.* Yangjiang, China 12 July – 3 August 2010, WMO/TD–No. 1580. Retrieved from http://www.wmo.int/pages/prog/www/IMOP/publications-IOM-series.html

Nash, J., Smout, R., Oakley, T., Pathack, B., & Kurnosenko, S. (2006). *WMO intercomparison of high quality radiosonde systems, Mauritius February 2005*. WMO/TD–No. 1303, p. 115. Retrieved from http://www.wmo.int/pages/prog/www/IMPO/publications/IOM-83_RSO-Mauritius/IOM-83_Radiosondes_Vacoas2005.pdf

Newell, R. E., Thouret, V., Cho, J. Y. N., Stoller, P., Marenco, A., & Smit, H. G. (1999). Ubiquity of quasi horizontal layers in the troposphere. *Nature*, *398*, 316–319. https://doi.org/10.1038/18642

Newell, R. E., Zhu, Y., Browell, E. V., Read, W. G., & Waters, J. W. (1996). Walker circulation and tropical upper tropospheric water vapor. *Journal of Geophysical Research*, *101*, 1961–1974.

Newton, R., Vaughan, G., Ricketts, H. M. A., Pan, L. L., Weinheimer, A. J., & Chemel, C. (2016). Ozonesonde profiles from the West Pacific Warm Pool: Measurements and validation. *Atmospheric Chemistry and Physics*, *16*, 619–634. https://doi.org/10.5194/acp-16-619-2016

O'Connor, F. M., Vaughan, G., & Murphy, G. (1998). Box and pump temperature measurements and the possible bias between Science Pump Corporation and ENSCI-type sondes, Polar stratospheric ozone 1997. *EC Air Pollution Report*, *66*, 712–715.

Oltmans, S. J., Lefohn, A. S., Harris, J. M., Galbally, I., Scheel, H. E., Bodeker, G., et al. (2006). Long-term changes in tropospheric ozone. *Atmospheric Environment*, *40*, 3156–3173.

Oltmans, S. J., Lefohn, A. S., Shadwick, D., Harris, J. M., Scheel, H. E., Galbally, I., et al. (2013). Recent tropospheric ozone changes – A pattern dominated by slow or no growth. *Atmospheric Environment*, *67*, 221–351. https://doi.org/10.1016/j.atmosenv.2012.10.057

Paneth, F. A., & Glückauf, E. (1941). Measurement of atmospheric ozone by a quick electrochemical method. *Nature*, *147*, 614–615.

Parrington, M., Palmer, P. I., Henze, D. K., Tarasick, D. W., Hyer, E. J., Owen, R. C., et al. (2012). The influence of boreal biomass burning emissions on the distribution of tropospheric ozone over North America and the North Atlantic during 2010. *Atmospheric Chemistry and Physics*, *12*, 2077–2098. https://doi.org/10.5194/acp-12-2077-2012

Petzold, A., Thouret, V., Gerbig, C., Zahn, A., Brenninkmeijer, C. A. M., Gallagher, M. H., et al. (2015). Global-scale atmosphere monitoring by in-service aircraft – Current achievements and future prospects of the European Research Infrastructure IAGOS. *Tellus B: Chemical and Physical Meteorology*, *67*, 1–24. https://doi.org/10.3402/tellusb.v67.28452

Pitts, J. N., McAfee, J. M., Long, W. D., & Winer, A. M. (1976). Long-path infrared spectroscopic investigation at ambient concentrations of the 2% neutral buffered potassium iodide method for determination of ozone. *Environmental Science and Technology*, *10*(8), 787–793.

Proffitt, M. H., & McLaughlin, R. J. (1983). Fast response dual-beam UV-absorption photometer suitable for use on stratospheric balloons. *Review of Scientific Instruments*, *54*, 1719–1728.

Randel, W., & Thompson, A. M. (2011). Interannual variability and trends in tropical ozone derived from SAGE II satellite data and SHADOZ ozonesondes. *Journal of Geophysical Research*, *116*, D07303. https://doi.org/10.1029/2010JD015195

Randel, W. F., & Wu, F. (1999). A stratospheric ozone trends data set for global modeling studies. *Geophysical Research Letters*, *26*, 3089–3092. https://doi.org/10.1029/1999GL900615

Rosen, J. (1968). Simultaneous dust and ozone soundings over North and central America. *Journal of Geophysical Research*, *73*(2), 479–486. https://doi.org/10.1029/JB073i002p00479

Saltzman, B. E., & Gilbert, N. (1959). Iodometric microdetermination of organic oxidants and ozone. Resolution of mixtures by kinetic colourimetry. *Analytical Chemistry*, *31*, 1914–1920.

Saltzman, B. E., & Wartburg, A. F. (1965). Absorption Tube for Removal of Interfering Sulfur Dioxide in Analysis of Atmospheric Oxidant. *Anal. Chem.*, *37*, 6, 779–782, https://doi.org/10.1021/ac60225a047

Schenkel, A., & Broder, B. (1982). Interference of some trace gases with ozone measurements by the KI method. *Atmospheric Environment*, *16*, 2187–2190.

Smit, H. G. J. & ASOPOS Panel. (2014). *Quality assurance and quality control for ozonesonde measurements in GAW, WMO Global Atmosphere*. Watch report series, No. 121, p. 100. Geneva: World Meteorological Organization. GAW Report No. 201. Retrieved from https://library.wmo.int/pmb_ged/gaw_201_en.pdf

Smit, H. G. J., & Kley, D. (1998). *JOSIE: The 1996 WMO International intercomparison of ozonesondes under quasi flight conditions in the environmental simulation chamber at Jülich*. Geneva: World Meteorological Organization. WMO Global Atmosphere Watch Report No. 130, WMO TD No. 926.

Smit, H. G. J., Oltmans, S., Deshler, T., Tarasick, D., Johnson, B., Schmidlin, F., et al. (2012). *SI2N/O3S-DQA activity: Guidelines for homogenization of ozone sonde data, Activity as part of SPARC-IGACO-IOC Assessment (SI2N)*. Past Changes in the Vertical Distribution OF Ozone Assessment 2012. Retrieved from http://www943das.uwyo.edu/%7Edeshler/NDACC_O3Sondes/O3s_DQA/O3S-DQA944Guidelines%20Homogenization-V2-19November2012.pdf

Smit, H. G. J., Straeter, W., Johnson, B., Oltmans, S., Davies, J., Tarasick, D. W., et al. (2007). Assessment of the performance of ECC-ozonesondes under quasi-flight conditions in the environmental simulation chamber: Insights from the Juelich Ozone Sonde Intercomparison Experiment (JOSIE). *Journal of Geophysical Research*, *112*, D19306. https://doi.org/10.1029/2006JD007308

Smit, H. G. J., & Straeter, W. (2004). *JOSIE-2000, Jülich Ozone Sonde Intercomparison Experiment 2000, The 2000 WMO international intercomparison of operating procedures for ECC-ozonesondes at the environmental simulation facility at Jülich.* WMO Global Atmosphere Watch report series, No. 158 (Technical Document No. 1225). Geneva: World Meteorological Organization.

Smit, H. G. J., Sträter, W., Helten, M., & Kley, D. (2000). *Environmental simulation facility to calibrate airborne ozone and humidity sensors. Jül Berichte Nr 3796.* Germany: Forschungszentrum Jülich.

Smit, H. G. J., Sträter, W., Kley, D., & Profitt, M. H. (1994). The evaluation of ECC-ozonesondes under quasi flight conditions in the environmental simulation chamber at Jülich. In P. M.Borell, et al. (Eds.), *Proceedings of Eurotrac symposium 1994* (pp. 349–353). The Hague, The Netherlands: SPB Academic Publishing bv.

Smit, H. G. J., Thompson, A. M., & ASOPOS Panel. (2020). ASOPOS 2.0: Assessment of Standard Operating Procedures for Ozone Sondes, WMO/GAW Report, in press.

SPARC-IOC-GAW. (1998). *Assessment of Trends in the Vertical Distribution of Ozone: SPARC Report No. 1, WMO Global Ozone Research and Monitoring Project Report No. 43.* Geneva: World Meteorological Organization.

Staehelin, J., Harris, N., Appenzeller, C., & Eberhard, J. (2001). Ozone trends: A review. *Reviews of Geophysics*, *39*(2), 231–290. https://doi.org/10.1029/1999RG000059

Staufer, J., Staehelin, J., Stübi, R., Peter, T., Tummon, F., & Thouret, V. (2013). Trajectory matching of ozonesondes and MOZAIC measurements in the UTLS – Part 1: Method description and application at Payerne, Switzerland. *Atmospheric Measurement Techniques*, *6*, 3393–3406. https://doi.org/10.5194/amt-6-3393-2013

Staufer, J., Staehelin, J., Stübi, R., Peter, T., Tummon, F., & Thouret, V. (2014). Trajectory matching of ozonesondes and MOZAIC measurements in the UTLS – Part 2: Application to the global ozonesonde network. *Atmospheric Measurement Techniques*, *7*, 241–266. https://doi.org/10.5194/amt-7-241-2014

Stauffer, R. M., Morris, G. A., Thompson, A. M., Joseph, E., Coetzee, G. J. R., & Nalli, N. R. (2014). Propagation of radiosonde pressure sensor errors to ozonesonde measurements. *Atmospheric Measurement Techniques*, *7*(1), 65–79. https://doi.org/10.5194/amt-7-65-2014

Stauffer, R. M., Thompson, A. M., Kollonige, D. E., Witte, J. C., Tarasick, D. W., Davies, J., et al. (2020). A post-2013 dropoff in total ozone at a third of global ozonesonde stations: Electrochemical concentration cell instrument artifacts?*Geophysical Research Letters*, *47*, e2019GL086791. https://doi.org/10.1029/2019GL086791

Stauffer, R. M., Thompson, A. M., & Witte, J. C. (2018). Characterizing global ozonesonde profile variability from surface to the UT/LS with a clustering technique and MERRA-2 reanalysis. *Journal of Geophysical Research: Atmospheres*, *123*, 6213–6229. https://doi.org/10.1029/2018JD028465

Steinbrecht, W, Claude, H., Schönenborn, F., Leiterer, U., Dier, H., & Lanzinger, E. (2008). Pressure and temperature differences between Vaisala RS80 and RS92 radiosonde systems. *Journal of Atmospheric and Oceanic Technology*, *25*, 909–927. https://doi.org/10.1175/2007JTECHA999.1

Steinbrecht, W., Schwarz, R., & Claude, H. (1998). New pump correction for the Brewer-Mast ozone sonde: Determination from experiment and instrument intercomparisons. *Journal of Atmospheric and Oceanic Technology*, *15*, 144–156. https://doi.org/10.1175/1520-0426(1998)015<0144:NPCFTB>2.0.CO

Sterling, C. W., Johnson, B. J., Oltmans, S. J., Smit, H. G. J., Jordan, A. F., Cullis, P. D., et al. (2018). Homogenizing and estimating the uncertainty in NOAA's long -term vertical ozone profile records measured with the electrochemical concentration cell ozonesonde. *Atmospheric Measurement Techniques*, *11*, 3661–3687. https://doi.org/10.5194/amt-11-3661-2018

Tanimoto, H., Zbinden, R. M., Thouret, V., & Nédélec, P. (2015). Consistency of tropospheric ozone observations made by different platforms and techniques in the global databases. *Tellus B: Chemical and Physical Meterology*, *67*, 27073. https://doi.org/10.3402/tellusb.v67.27073

Tarasick, D. W., Carey-Smith, T. K., Hocking, W. K., Moeini, O., He, H., Liu, J., et al. (2019). Quantifying stratosphere-troposphere transport of ozone using balloon-borne ozonesondes, radar windprofilers and trajectory models. *Atmospheric Environment*, *198*(2019), 496–509. https://doi.org/10.1016/j.atmosenv.2018.10.040

Tarasick, D. W., Davies, J., Anlauf, K., & Watt, M. (2000). Response of ECC and Brewer-Mast ozonesondes to sulfur dioxide interference. *Proceedings of Quadrennial Ozone Symposium 2000* (pp. 675–676). Sapporo, Japan: National Space Development Agency of Japan.

Tarasick, D. W., Davies, J., Anlauf, K., Watt, M., Steinbrecht, W., & Claude, H.J. (2002). Laboratory investigations of the response of Brewer-Mast sondes to tropospheric ozone. *Journal of Geophysical Research*, *107*, D16. https://doi.org/10.1029/2001JD001167

Tarasick, D. W., Davies, J., Smit, H. G. J., & Oltmans, S. J. (2016). A re-evaluated Canadian ozonesonde record: Measurements of the vertical distribution of ozone over Canada from 1966 to 2013. *Atmospheric Measurement Techniques*, *9*, 195–214. https://doi.org/10.5194/amt-9-195-2016

Tarasick, D. W., Fioletov, V. E., Wardle, D. I., Kerr, J. B., & Davies, J. (2005). Changes in the vertical distribution of ozone over Canada from ozonesondes: 1980-2001. *Journal of Geophysical Research*, *110*, D02304. https://doi.org/10.1029/2004JD004643

Tarasick, D. W., Galbally, I., Cooper, O. R., Schultz, M. G., Ancellet, G., LeBlanc, T., et al. (2019). TOAR-observations: Tropospheric ozone from 1877 to 2016, observed levels, trends and uncertainties. *Elementa: Science of the Anthropocene*, *7*(1), 39. http://doi.org/10.1525/elementa.376

Tarasick, D. W., Jin, J. J., Fioletov, V. E., Liu, G., Thompson, A. M., Oltmans, S. J., et al. (2010). High-resolution tropospheric ozone fields for INTEX and ARCTAS from IONS ozonesondes. *Journal of Geophysical Research*, *115*, D20301. https://doi.org/10.1029/2009JD012918

Terao, Y., & Logan, J. A. (2007). Consistency of time series and trends of stratospheric ozone as seen by ozonesonde, SAGE II, HALOE, and SBUV(/2). *Journal of Geophysical Research*, *112*, D06310. https://doi.org/10.1029/2006JD007667

Thompson, A. M., Miller, S. K., Tilmes, S., Kollonige, D. W., Witte, J. C., Oltmans, S. J., et al. (2012). Southern Hemisphere Additional Ozonesondes (SHADOZ) ozone climatology (2005–2009): Tropospheric and tropical tropopause layer (TTL) profiles with comparisons to OMI-based ozone products. *Journal of Geophysical Research*, *117*, D23301. https://doi.org/10.1029/2011JD016911

Thompson, A. M., Oltmans, S. J., Tarasick, D. W., von der Gathen, P., Smit, H. G. J., & Witte, J. C (2010). Strategic ozone sounding networks: Review of design and accomplishments. *Atmospheric Environments*, *45*, 2145–2163.

Thompson, A. M., Smit, H. G. J., Witte, J. C., Stauffer, R. M., Johnson, B. J., Morris, G., et al. (2019). Ozonesonde quality assurance: The JOSIE-SHADOZ (2017) experience. *Bulletin of the American Meteorological Society*, *100*(1), 155–171.

Thompson, A. M., Stauffer, R. M., Witte, J. C., & Kollonige, D. W. (2020). The role of convection in tropical ozone trends (1998-2018) based on SHADOZ profiles, Earth and Space Science Open Archive, https://doi.org/10.1002/essoar.10503415.1

Thompson, A. M., Stone, J. B., Witte, J. C., Miller, S. K., Oltmans, S. J., Kucsera, T. L., et al. (2007). Intercontinental Chemical Transport Experiment Ozonesonde Network Study (IONS) 2004: 2. Tropospheric ozone budgets and variability over northeastern North America. *Journal of Geophysical Research*, *112*, D12S13. https://doi.org/10.1029/2006JD007670

Thompson, A. M., Stone, J. B., Witte, J. C., Pierce, R. B., Chatfield, R. B., Oltmans, S. J., et al. (2007). Intercontinental Chemical Transport Experiment Ozonesonde Network Study (IONS) 2004: 1. Summertime upper troposphere/lower stratosphere ozone over northeastern North America. *Journal of Geophysical Research*, *112*, D12S12. https://doi.org/10.1029/2006JD007441

Thompson, A. M., Witte, J. C., McPeters, R. D., Oltmans, S. J., Schmidlin, F. J., Logan, J. A., et al. (2003). Southern Hemisphere Additional Ozonesondes (SHADOZ) 1998-2000 tropical ozone climatology 1. Comparison with Total Ozone Mapping Spectrometer (TOMS) and ground-based measurements. *Journal of Geophysical Research*, *108*, 8238. https://doi.org/10.1029/2001JD000967

Thompson, A. M., Witte, J. C., Sterling, C. W., Jordan, A., Johnson, B. J., Oltmans, S. J., et al. (2017). First reprocessing of Southern Hemisphere Additional Ozonesondes (SHADOZ) Ozone Profiles (1998-2016). 2. Comparisons with satellites and ground-based instruments. *Journal of Geophysical Research: Atmospheres*, *122*, 13000–13025. https://doi.org/10.1002/2017JD027406

Thornton, D. C., & Niazy, N. (1982). Sources of background current in the ECC ozonesonde: Implications for total ozone measurements. *Journal of Geophysical Research*, *87*, 8943–8950.

Thornton, D. C., & Niazy, N. (1983). Effects of solution mass transport on the ECC ozonesonde background current. *Geophysical Research Letters*, *10*, 148–151.

Thouret, V., Cammas, J.-P., Sauvage, B., Athier, G., Zbinden, R., Nédélec, P., et al. (2006). Tropopause referenced ozone climatology and inter-annual variability (1994–2003) from the MOZAIC programme. *Atmospheric Chemistry and Physics*, *6*, 1033–1051. https://doi.org/10.5194/acp-6-1033-2006

Thouret, V., Marenco, A., Logan, J. A., Nédélec, P., & Grouhel, C. (1998). Comparisons of ozone measurements from the MOZAIC airborne program and the ozone sounding network at eight locations. *Journal of Geophysical Research*, *103*(D19), 25695–25720. https://doi.org/10.1029/98JD02243

Torres, A. (1981). *ECC performance at high altitudes: Pump efficiency*. NASA Tech. Memo., TM93290.

Van Malderen, R., Allaart, M. A. F., De Backer, H., Smit, H. G. J., & De Muer, D. (2016). On instrumental errors and related correction strategies of ozonesondes: Possible effect on calculated ozone trends for the nearby sites Uccle and De Bilt. *Atmospheric Measurements Techniques*, *9*, 3793–3816. https://doi.org/10.5194/amt-9-3793-2016

Van Malderen, R., De Backer, H., Delcloo, A., & Allaart, M. (2014). Identifying the origin of anomalous high tropospheric ozone in the ozonesonde data at Uccle by comparison with nearby De Bilt. *Atmosphere-Ocean*, *53*, 102–116. https://doi.org/10.1080/07055900.2014.886552

Vassy, A. (1958). Appareil enregistreur donnant la concentration de l'ozone dans l. air. *Geofisica Pura e Applicata*, *39*, 164. https://doi.org/10.1007/BF02001142

Vömel, H., & Diaz, K. (2010). Ozone sonde cell current measurements and implications for observations of near-zero ozone concentrations in the tropical upper troposphere. *Atmospheric Measurements Techniques*, *3*, 495–505. https://doi.org/10.5194/amt-3-495-2010

Vömel, H., Smit, H. G. J., Tarasick, D., Johnson, B., Oltmans, S. J., Selkirk, H., et al. (2020). A new method to correct the ECC ozone sonde time response and its implications for "background current" and pump efficiency. *Atmospheric Measurements Techniques*, *13*, 5667–5680.

Volz, A., & Kley, D. (1988). Evaluation of the Montsouris series of ozone measurements made in the 19th century. *Nature*, *332*(6161), 240–242. https://doi.org/10.5194/amt-13-5667-2020

Von der Gathen, P., Rex, M., Harris, N. R. P., Lucic, D., Knudsen, B. M., Braathen, G. O., et al. (1995). Observational evidence for chemical ozone depletion over the Arctic winter 1991-92. *Nature*, *375*, 131–134.

Walker, K. A., Strong, K., Fogal, P. F., Drummond, J. R. & the Canadian Arctic ACE/OSIRIS Validation Campaign Team. (2016). *The Canadian Arctic ACE/OSIRIS Validation Project at PEARL: Validating Satellite Observations Over the High Arctic*. Geophysical Research Abstracts, Vol. 18, EGU2016-4837. EGU General Assembly.

Witte, J. C., Thompson, A. M., Schmidlin, F. J., Northam, E. T., Wolff, K. R., & Brothers, G. B. (2019). The NASA Wallops Flight Facility digital ozonesonde record: Reprocessing, uncertainties, and dual launches. *Journal of Geophysical Research: Atmospheres*, *124*, 3565–3582. https://doi.org/10.1029/2018JD030098

Witte, J. C., Thompson, A. M., Smit, H. G. J., Fujiwara, M., Posny, F., Coetzee, G. J. R., et al. (2017). First reprocessing of Southern Hemisphere ADditional OZonesondes (SHADOZ) profile records (1998-2015): 1. Methodology and evaluation. *Journal of Geophysical Research: Atmospheres*, *122*(12), 6611–6636. https://doi.org/10.1002/2016JD026403

Witte, J. C., Thompson, A. M., Smit, H. G. J., Vömel, H., Posny, F., & Stübi, R. (2018). First reprocessing of Southern Hemisphere ADditional OZonesondes profile records: 3. Uncertainty in ozone profile and total column. *Journal of Geophysical Research: Atmospheres*, *123*, 3243–3268. https://doi.org/10.1002/2017JD027791

WMO (World Meteorological Organization), Scientific Assessment of Ozone Depletion. (2014). *World Meteorological Organization*, Global Ozone Research and Monitoring. Project – Report No. 55, Geneva, p. 416.

WMO (World Meteorological Organization), Scientific Assessment of Ozone Depletion. (2018). Global Ozone Research and Monitoring Project-Report No. 58. Geneva, Switzerland, p. 588.

Zbinden, R. M., Thouret, V., Ricaud, P., Carminati, F., Cammas, J.-P., & Nédélec, P. (2013). Climatology of pure tropospheric profiles and column contents of ozone and carbon monoxide using MOZAIC in the mid-northern latitudes (24ºN to 50ºN) from 1994 to 2009. *Atmospheric Chemistry and Physics*, *13*, 12363–12388. http://dx.doi.org/10.5194/acp-13-12363-2013

Zerefos, C., Contopoulos, G., & Skalkeas, G. (Eds.). (2009). *Twenty years of ozone decline. Proceedings of the Symposium for the 20th Anniversary of the Montreal Protocol* (p. 470). Netherlands: Springer.

Erratum

In the originally published version of this article, there were errors in Equations (10) and (11). The equations have been updated and this may be considered the authoritative version of record.